JGR Oceans

RESEARCH ARTICLE
10.1029/2024JC021644

Influence of Freshwater Fluxes and Topography on the Distribution of Water Masses on the Antarctic Continental Shelf

Christopher Y. S. Bull[1,2], **David R. Munday**[3], **and Adrian Jenkins**[1]

[1]Department of Geography and Environmental Sciences, Northumbria University, Newcastle upon Tyne, UK, [2]Now at: Australia's Climate Simulator (ACCESS-NRI), Australian National University, Canberra, ACT, Australia, [3]British Antarctic Survey, Cambridge, UK

Key Points:

- An idealized ocean model is used to investigate the influence of changes in freshwater fluxes on shelf temperatures around Antarctica
- Both a positive uniform increase of freshwater or decrease in the meridional gradient of freshwater can lead to warmer waters on the shelf
- Freshening flux transported by the mean circulation drives large-scale density reorganization, allowing warmer waters to flow onto the shelf

Supporting Information:

Supporting Information may be found in the online version of this article.

Correspondence to:

C. Y. S. Bull,
chris.bull@anu.edu.au

Citation:

Bull, C. Y. S., Munday, D. R., & Jenkins, A. (2025). Influence of freshwater fluxes and topography on the distribution of water masses on the Antarctic continental shelf. *Journal of Geophysical Research: Oceans*, *130*, e2024JC021644. https://doi.org/10.1029/2024JC021644

Received 1 AUG 2024
Accepted 9 JUL 2025

Author Contributions:

Conceptualization: Christopher Y. S. Bull, David R. Munday, Adrian Jenkins
Formal analysis: Christopher Y. S. Bull
Funding acquisition: Adrian Jenkins
Methodology: Christopher Y. S. Bull, David R. Munday, Adrian Jenkins
Project administration: Adrian Jenkins
Supervision: David R. Munday
Visualization: Christopher Y. S. Bull
Writing – original draft: Christopher Y. S. Bull
Writing – review & editing: Christopher Y. S. Bull, David R. Munday, Adrian Jenkins

Abstract At the Antarctic coast, ice shelves flow from the ice sheet and are vulnerable to future changes in sub-surface ocean temperatures at the southern margins. A better understanding of how projected changes in freshwater fluxes drive the onshore transport of warm deep waters across the shelf break toward the ice shelves is needed. This study uses idealized ocean simulations to explore how changes in freshwater flux influence the temperature structure on Antarctica's shelf seas across Southern Ocean circulation regimes (throughflow or gyre—determined by basin geometry). We use idealized freshwater perturbations applied as a surface salt flux to disentangle the effects of spatially varying reduced sea ice from spatially uniform increases in precipitation. Overall, we find that reductions in sea ice and increases in precipitation both lead to warmer waters on the shelf across all flow regimes. A cross-slope density gradient threshold is identified which leads to warmer shelf temperatures. We also find that the large-scale circulation regime (throughflow or gyre) influences how susceptible the existing shelf temperatures are to changes in freshwater flux but this effect is less important than with wind changes. Whilst the overall tendency is for the shelf to warm under a uniform decrease in the salt flux, simulations with a throughflow on the shelf warm more strongly than simulations with a gyre on the shelf, this is due to a stronger meridional density gradient in the throughflow case. On the large-scale, imprints of the circulation regime manifest in temperature and salinity changes, driving the spatial pattern of change.

Plain Language Summary At the Antarctic margins, ice shelves are vulnerable to changes in sub-surface ocean temperatures. As the earth warms, the hydrological cycle is amplified, leading to freshening in the precipitation dominated Southern Ocean. At the same time, warming near-surface temperatures will lead to less sea ice annually. An open question is how these two kinds of changes are likely to affect the ocean temperatures close to Antarctica's ice shelves. In this study, we use an idealized ocean model to understand how possible precipitation and sea ice changes affect ocean temperatures near the ice shelves, across different regions of Antarctica. We find that uniform increases in freshwater and reductions in sea ice can both lead to warmer waters near the ice shelves across all regions. The key processes underlying these changes are described as follows, when salt is added to the shelf, it is destabilizing, the shelf mixes and becomes cold and salty. This water mass can then flow down the slope into the deep ocean. In contrast, when salt is removed, it stabilizes the surface water over the shelf, reducing vertical mixing and it becomes much easier for warm water offshore to move onto the shelf and warm it.

1. Introduction

Ice loss from the Antarctic Ice Sheet is the largest uncertainty in projections of future sea-level rise under global warming (Edwards et al., 2021). A central challenge lies in understanding the connection between future large-scale climate forcing and the changes in ocean properties in the vicinity of the Antarctic continent. Climate simulations suggest that future changes in buoyancy forcing will be more important than wind changes in determining the future Southern Ocean's temperature and salinity structure (Shi et al., 2020). Large-scale changes in the freshwater forcing of the Southern Ocean are already being observed (Durack & Wijffels, 2010; Jacobs et al., 2022). Future projections suggest enhanced surface freshening due to increased sea ice melt and precipitation (Cai et al., 2023; Purich & England, 2021). Annually, sea ice production and melt leads to a large-scale, re-distribution of freshwater with extraction of freshwater in the south and release in the north. A decline in annual sea ice and increase in precipitation, will thus modify the meridional buoyancy flux gradient. A clearer

understanding of how the sub-surface temperatures in the Antarctic margins will respond to a change in freshwater forcing is needed.

Past realistic configuration regional modeling studies have looked at how changes in surface freshwater fluxes influence warm water inflow onto Antarctica's shelf seas, increasing melt rates in the ice shelf cavities (Caillet et al., 2023; Haigh & Holland, 2024). Through a wide range of perturbations, many additional studies have found that changes in stratification near an ice front, lead to changes in available heat on the shelf (Bull et al., 2021; Daae et al., 2020; Haid et al., 2023; Morrison et al., 2023; Ong et al., 2025; Si et al., 2023). A common thread is that changes in freshwater fluxes modify the cross-shelf break density gradient, enabling deep offshore warm waters to flow across the shelf break. Simulations with idealized perturbations but realistic geometry suggest regionally varying responses to freshwater perturbations (Haid et al., 2023; Moorman et al., 2020), suggesting further work is needed in understanding why different regions respond differently. One possible factor for the different regional responses, is the complex combination of flow regimes (throughflow or gyre; gyre regimes form where f/h gradients are sufficiently steep to block throughflow) that exists in the Southern Ocean (Sonnewald et al., 2023). Some theory (below) suggests that these two regimes may respond differently to a change in freshwater flux gradient compared to a uniform magnitude change. An idealized approach that considers the Southern Ocean's unique geometry could be used to test this possibility.

The Antarctic Slope Front (ASF) on the continental shelf break modulates onshore heat transport associated with inflow of warmer sub-surface waters. The ASF is located amongst a complex Southern Ocean circulation, with both mixtures of throughflow and gyre regimes, where the buoyancy fluxes and surface stress drive the ocean circulation. Throughflow regime currents are the eastward flowing Antarctic Circumpolar Current (ACC) and a shelf confined westward Antarctic Slope Current (ASC). The ACC is driven by wind and buoyancy forcing and is the world's strongest current, in terms of volume transport (Hogg, 2010; Olbers et al., 2012). Recent observations suggest the ACC has shown little change to increases in wind strength, which is consistent with it being eddy saturated (Gutierrez-Villanueva et al., 2023). There is evidence that it may be accelerating due to ocean warming (Shi et al., 2021). However, it is unclear whether this is an acceleration of the ACC or a southward shift of the eastward flow in subtropical gyres (Stewart, 2021). Gyre regimes are characterized by the clockwise circulating Weddell, Ross, and Australian-Antarctic Gyres (Patmore, 2019). Historically, surface wind stress curl has been related to the depth-integrated transport of gyres (Stommel, 1948; Sverdrup, 1947) with meridional gradients of buoyancy fluxes as a means to modulate gyre transport (Bhagtani et al., 2023; Colin de Verdière, 1989; Hogg & Gayen, 2020; Holland, 1973; Liu et al., 2022). Such gradients are potentially more relevant to the Southern Ocean (Gray & Riser, 2014; Neme et al., 2023). The above theories suggest that both throughflow and gyre regimes can be modulated by a change in the meridional buoyancy gradient. It is also plausible that a uniform change in the magnitude of freshwater forcings is relevant. For example, it is believed that the Bellingshausen sea is warm because the freshwater input from precipitation is too great, and salt input from winter sea ice growth relatively too small, to allow convection (Talbot, 1988). Suppose in this instance that the precipitation were reduced and sea ice production increased, then would the Bellingshausen shift into a cold regime? How can we disentangle the effects of projected precipitation and sea ice change?

Bull et al. (2025, hereafter B25) examined the influence of topography and winds in determining Antarctica's shelf water properties. B25 found that a constant offset in the winds (westerly winds shift south and intensify) led to warmer waters on the shelf. The circulation regime (throughflow or gyre—determined by basin geometry), additionally influenced the mean shelf temperature and how susceptible the existing shelf temperatures are to changes in surface stress. B25 re-visited a well-known distinction between gyre and throughflow regimes. In the case of a gyre regime (a barotropic closed box with a meridional gradient in the wind), a constant offset in the wind does not alter the horizontal circulation. However, in the case of a throughflow regime (a barotropic re-entrant box with a uniform wind), a constant offset in the wind will have a dramatic effect on the circulation, namely the wind offset accelerates the flow. A natural question in the present study is, given that gyre regimes are influenced by meridional gradients in freshwater, does the same response occur (as the wind case) when forced by a uniform offset in freshwater? This study then is intended as a freshwater analogue of the experiment design to B25.

The goal of this study is to re-visit channel and gyre regimes in the context of an idealized Southern Ocean model with changes in freshwater forcings that are expected in a warming climate. The community, for the purpose of attribution, needs to understand the implications of a change in the gradient of freshwater fluxes compared to a

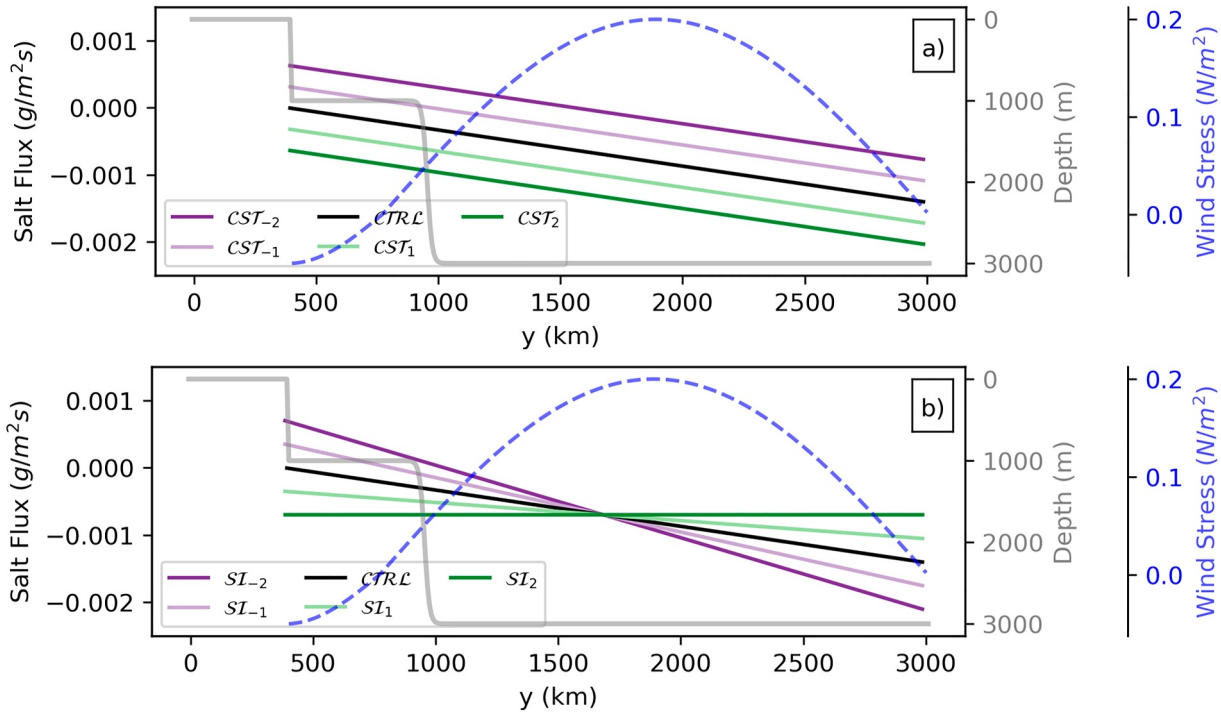

Figure 1. Nine zonally uniform salt flux forcings applied to each of the 3 bathymetries (Figure 2), all experiments are listed in Table 2. Black is the control simulation and perturbation experiments are created by either: (a) adding a uniform constant offset (1–15; Table 2) or (b) changing the meridional gradient "SI" (16–30; Table 2). The control simulation ($\mathcal{CTRL}$) is the same across both experiment sets (a, b). Dashed faint blue (τ_0) shows the zonally uniform wind stress and gray line shows the shelf and sea floor bathymetry common to all experiments (both on twin axis, scale on right). Positive salt flux numbers suggest salt entering the ocean surface.

change in the magnitude; this paper looks to make progress toward disentangling these issues. We believe this is the first time an incremental mixture of circulation regimes with distinct gradient and offset forcings has been used to study the temperature structure on the shelf. Two questions arise:

1. Can changes in cross-slope freshwater gradients or changes in the total amount of precipitation significantly affect shelf temperatures?
2. Like B25, is basin geometry important for modulating shelf temperature changes with freshwater changes?

The paper is presented as follows. Section 2 describes key model parameters and the experiment design, results in Section 3 and a discussion in Section 4.

2. Model and Experimental Design

This study uses an idealized Southern Ocean channel model inspired by similar previous studies (e.g., Abernathey et al., 2011; Morrison et al., 2011), where the interest is to have a simple system in which to understand the freshwater flux's role in setting shelf properties without coupled momentum and feedback effects from a coupled sea ice model. A key requirement is the ability to create different flow regimes by modifying the boundary condition (domain geometry or bathymetry, see discussion in Section 2.2). Figures 1 and 2 shows the surface forcing and bathymetry, Figure 3 is a 3D schematic snapshot of the model configuration with control forcing and a south-north wall at $x = 405$ km, this leads to gyre regimes on the shelf and deep ocean (see Section 2.2 for further details). The modeling configuration and experiment design used here is very similar to B25, the difference being the restoring conditions and surface salt flux. The bathymetries used are the same as B25 except only three of them are used (Section 2.2 and Figure 2).

2.1. NEMO Model Configuration

The ocean general circulation model used in this study is version 4.0.4 of the Nucleus for European Modeling of Ocean model (NEMO; Madec et al., 2019). NEMO solves the incompressible, Boussinesq, hydrostatic primitive

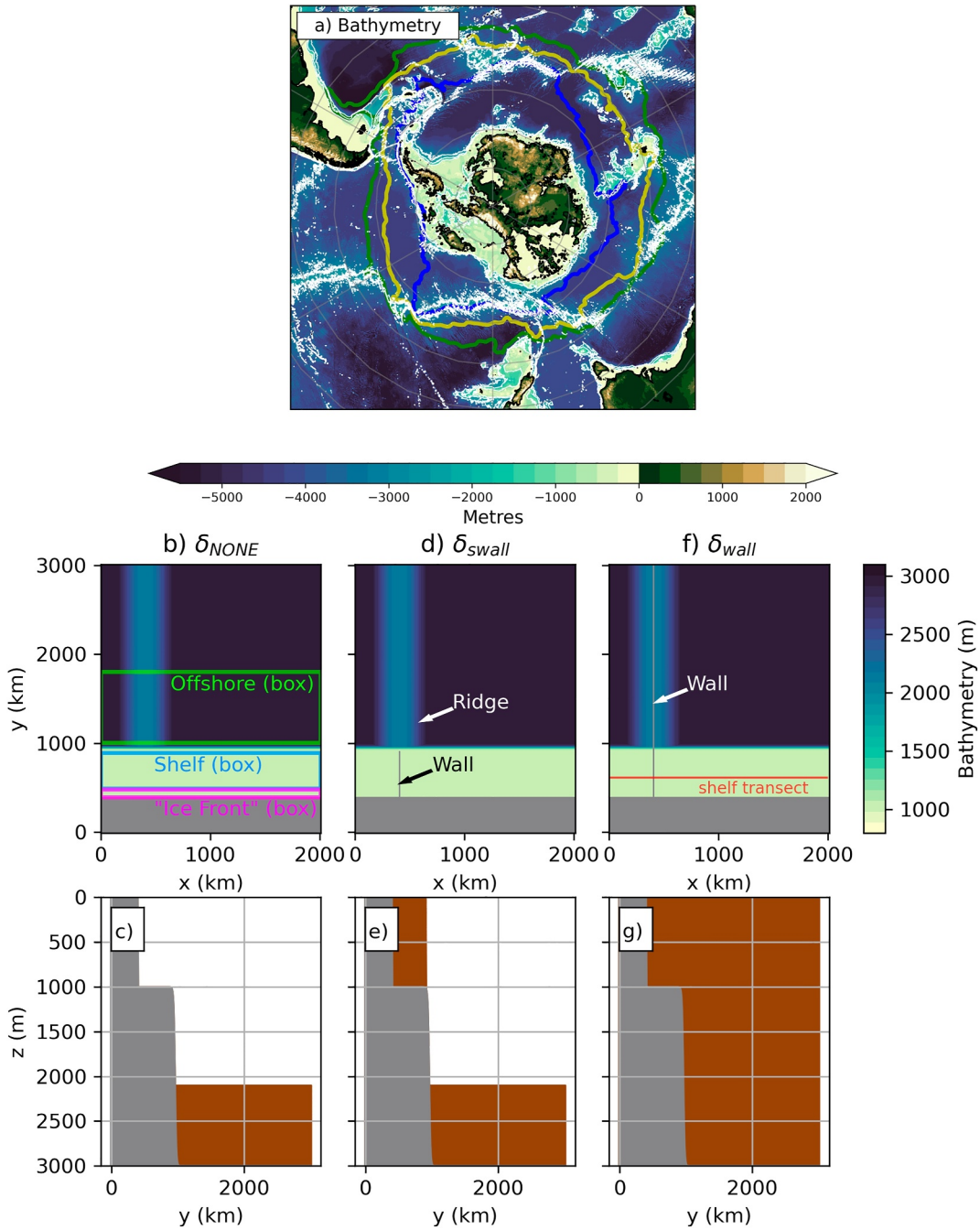

Figure 2. (a) ETOPO1 bathymetry, thick contours indicate Southern Boundary (blue), Polar Front (yellow), and Subantarctic Front (green) from Park et al. (2019); thin white contours highlight −3,000 m, −2,000 m, −1,000 m isobaths, and black contour is the surface land mask. (b–g) Each column is a new bathymetry where the three different bathymetries ($\delta_{\text{NONE}}, \delta_{\text{swall}}, \delta_{\text{wall}}$) create different "boundary conditions." Second row: plan view. Third row: meridional slice where gray shows the bathymetry (unchanged across all bathymetries) and brown shading shows the wall at $x = 405$ km (approx). Regions labeled "Offshore (box)" (lime), "Shelf (box)" (blue) and "Ice Front" (box) (magenta) in panel b, are used for diagnostics in Figure 9. "Shelf transect" used for shelf related diagnostics indicated in red, panel (f).

equations with a split-explicit free-surface formulation. NEMO here uses a z*-coordinate (varying cell thickness) C-grid with partial cells at the bottom-most ocean levels in order to provide a more realistic representation of bathymetry (Bernard et al., 2006). Our model settings include: a 55-term polynomial approximation of the reference Thermodynamic Equation of Seawater (TEOS-10; IOC, SCOR and IAPSO, 2010), nonlinear bottom

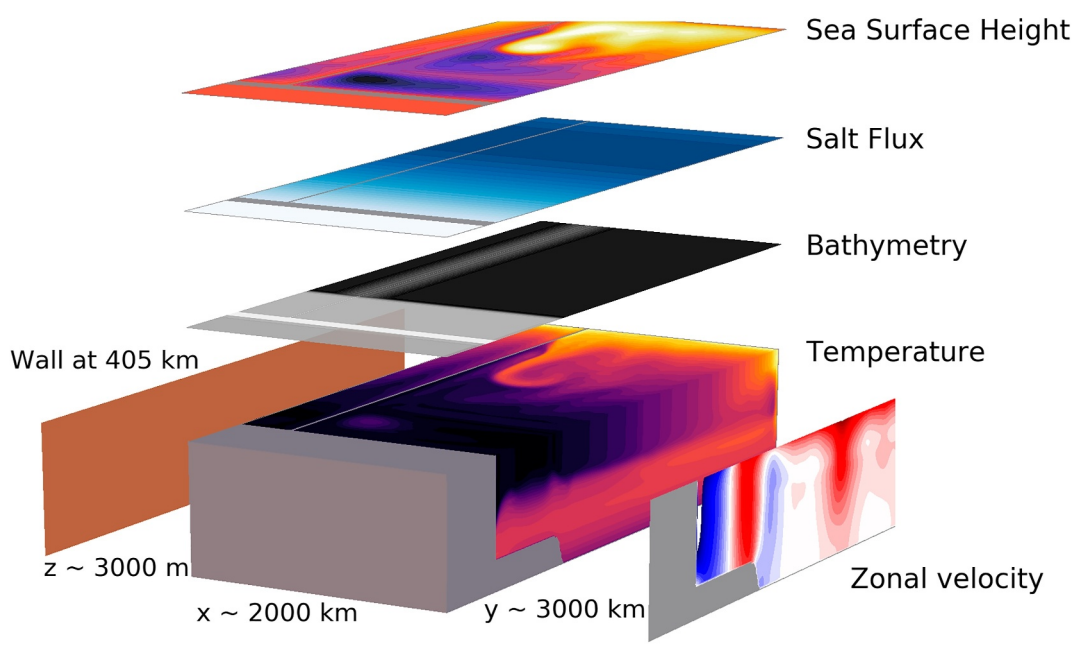

Figure 3. Configuration schematic that illustrates the model domain, mean circulation and surface forcing. A 3D snapshot of the model's temperature field from a single experiment with $\mathcal{CTRL}$ forcing (see Figure 1). The temperatures range from −1.9 to 1.5°C (black to warm colors). Overlaid, above: sea surface height (−5 to 20 cm; black to yellow), salt flux (blues indicates a fresh flux) and bathymetry (darker values are deeper); right: zonal mean zonal velocity (−20 to 20 cm/s; blue to red); left: most experiments have some kind of wall at 405 km rising from either the shelf or deep ocean ridge, here, there is a wall the full length of the domain. Note the vertical scale is stretched.

friction, a free-slip condition at the lateral boundaries, energy- and enstrophy-conserving momentum advection scheme and a prognostic turbulent kinetic energy scheme for vertical mixing. Laterally, we have spatially varying eddy coefficients (according to local mesh size) with a Laplacian operator for iso-neutral diffusion of tracers and a biharmonic operator for lateral diffusion of momentum.

Table 1 summarizes the modeling configuration where the surface forcing is detailed in Section 2.2. The modeling domain is on a β-plane with 257 × 385 regularly spaced grid boxes in x and y, respectively. The horizontal resolution of 7.9 km used here is "eddy permitting," meaning the resolution is unable to resolve the fastest-growing baroclinic modes (Hallberg, 2013). This resolution is slightly coarser than some models such as

Table 1
Key Parameters Used in the Configuration With Control Salt Flux

Symbol	Value	Description
L_x, L_y	$2,004, 3,025$ (km)	Domain size
H	$3,047$ (m)	Depth of domain
Δ_x, Δ_y	7.9 (km)	Horizontal resolution
Δ_z	1 (m) surface–135 (m) depth	Vertical resolution
f_0	$-1.46 * 10^{-4}$ (rad s^{-1})	Southern boundary Coriolis parameter
f_y	$-1.28 * 10^{-4}$ (rad s^{-1})	Northern boundary Coriolis parameter
L_{EW}	770 (km)	Value of y where winds transition from easterly to westerly
SFX_S, SFX_N	$0.0, -0.0014$ $(\text{g/m}^2\text{s})$	Control salt flux at southern (maximum) and northern boundary (minimum)
τ_E, τ_w	$-0.05, 0.2$ (N m^{-2})	Peak easterly and westerly wind stress
eiv	$2,000$ (m^2/s)	GM constant Eddy Induced Velocity (eiv) parameterisetion

(Abernathey et al., 2011), which used a resolution of 5 km. Having said this, our domain is larger than previous studies (2,000 × 3,000 km) and the scientific focus was on first-order effects; we needed an inexpensive configuration to enable the many sensitivity tests that were completed for this work. Recent work by others (e.g., Si et al., 2023), suggests that a resolution of 1 km is needed to completely capture the eddy driven cross slope heat transport, although we note the results do not qualitatively differ beyond 2 km. Another example is in Wilson et al. (2022), they use a resolution of ∼9.4 km/∼4.7 km (longitude/latitude) where sensitivity tests down to 5 km and found that "the key conclusions of this study remain unchanged." As a compromise, we use the Gent-McWilliams Eddy Parameterization (GM; Gent & Mcwilliams, 1990; Gent et al., 1995) to represent the effects of unresolved mesoscale eddies on tracer distribution, that is, temperature, salinity and other tracers. We choose $eiv = 2,000\ \mathrm{m}^2/\mathrm{s}$ based on Allison et al. (2011) and Visbeck et al. (1997). Sensitivity tests completed for B25 found that the behavior of the setup was largely unchanged with and without GM and so we feel that the compromise of coarse resolution here is acceptable given the large number of experiments.

The ocean floor is limited to 3, 023 m and is represented by 61 vertical levels, where the vertical grid spacing is ∼1 m at the surface and 135 m at the lowest level. Walls exist on the northern and southern boundaries in all experiments. The western-eastern boundary is fully re-entrant but in some cases is effectively blocked due to a wall at 405 km (Figure 2h). The simulations are initialized from rest with initial conditions derived from World Ocean Atlas 2018 (WOA; Boyer et al., 2018). The external forcing is a restoring condition (toward the initial state) at both the northern boundary and near surface for temperature, additionally, there is a surface wind stress (Figures 1a and 1b).

2.2. Experiments

The base configuration is identical to B25 except with near-surface salinity restoring turned off (northern boundary salinity restoring is kept on) and a salt flux applied at the surface. The forcing and boundary conditions consist of:

1. An initial and restoring condition based on World Ocean Atlas 2018:
   a. At the northern boundary for temperature and salinity,
   b. At the near surface for temperature.
2. A surface wind stress (Figures 1a and 1b).
3. Changing boundary conditions in the form of a wall at $x = 405$ km (Figures 2b–2g).
4. Salt flux applied at the surface to emulate precipitation or evaporation, sea ice growth or melt (Figures 1a and 1b).

In this study, the experiments are designed to highlight the dependence of the strength and location of the ASF to changes in flow regimes (boundary conditions) and changes in freshwater forcing. Perturbation experiments are created through modifying the salt flux at the surface and boundary condition (bathymetry), all experiments are listed in Table 2.

The wind stress "τ_0" forcing (Figures 1a and 1b) is zonally symmetric (meridional wind stress is zero) and is intended to represent a zonal average of the Southern Ocean's easterlies and westerlies using a sin curve with peak values of $-0.05, 0.2\ \mathrm{N/m}^2$.

In this study our objective is to use idealized freshwater perturbations to disentangle the effects of reducing sea ice (modifying the meridional freshwater gradient) from uniform increases in precipitation. To diagnose a plausible annual control freshwater flux, we consider the ERA5 freshwater budget and NASA sea ice data as follows. The ERA5 data is used to diagnose the atmospheric component of the freshwater flux. The ERA5 freshwater budget shows net freshwater input over the Southern Ocean (Figure S1 in Supporting Information S1), this is consistent with other studies, for example Figure 5 in Babu et al. (2018). Focusing on latitudes that are consistent with the restoring used (south of the Subantarctic Front, green line in Figure 2a). Over most of the Southern Ocean (50°S to ∼70°S), net precipitation is almost constant. From Figure S1a in Supporting Information S1 then, we take a value of $-2 \times 10^{-5}\ \mathrm{kg\ m^{-2}\ s^{-1}}$ for our control precipitation ($7 \times 10^{-4}\ \mathrm{g\ m^{-2}\ s^{-1}}$ salt flux).

In the annual integral, sea ice re-distributes freshwater and does not lead to a net change in the total freshwater/salinity. As we are interested in the annual freshwater flux with no seasonal cycle, the flux we are looking to emulate should average to zero—removing freshwater in the south where the sea ice is grown and producing

Table 2
List of Experiments

Number	Name	Boundary condition			Salt flux (g/m^{2}s)	
		Fully open	Shelf block	Fully closed	Max (southern boundary)	Min (northern boundary)
1	$\delta_{\text{NONE}}\mathcal{CST}_{-2}$	✓			0.0006	−0.0008
2	$\delta_{\text{NONE}}\mathcal{CST}_{-1}$	✓			0.0003	−0.0011
3	$\delta_{\text{NONE}}\mathcal{CTRL}$	✓			0.0	−0.0014
4	$\delta_{\text{NONE}}\mathcal{CST}_{1}$	✓			−0.0003	−0.0017
5	$\delta_{\text{NONE}}\mathcal{CST}_{2}$	✓			−0.0006	−0.002
6	$\delta_{\text{swall}}\mathcal{CST}_{-2}$		✓		0.0006	−0.0008
7	$\delta_{\text{swall}}\mathcal{CST}_{-1}$		✓		0.0003	−0.0011
8	$\delta_{\text{swall}}\mathcal{CTRL}$		✓		0.0	−0.0014
9	$\delta_{\text{swall}}\mathcal{CST}_{1}$		✓		−0.0003	−0.0017
10	$\delta_{\text{swall}}\mathcal{CST}_{2}$		✓		−0.0006	−0.002
11	$\delta_{\text{wall}}\mathcal{CST}_{-2}$			✓	0.0006	−0.0008
12	$\delta_{\text{wall}}\mathcal{CST}_{-1}$			✓	0.0003	−0.0011
13	$\delta_{\text{wall}}\mathcal{CTRL}$			✓	0.0	−0.0014
14	$\delta_{\text{wall}}\mathcal{CST}_{1}$			✓	−0.0003	−0.0017
15	$\delta_{\text{wall}}\mathcal{CST}_{2}$			✓	−0.0006	−0.002
16	$\delta_{\text{NONE}}\mathcal{SI}_{-2}$	✓			0.0007	−0.0021
17	$\delta_{\text{NONE}}\mathcal{SI}_{-1}$	✓			0.0003	−0.0018
18	$\delta_{\text{NONE}}\mathcal{CTRL}$	✓			0.0	−0.0014
19	$\delta_{\text{NONE}}\mathcal{SI}_{1}$	✓			−0.0004	−0.0011
20	$\delta_{\text{NONE}}\mathcal{SI}_{2}$	✓			−0.0007	−0.0007
21	$\delta_{\text{swall}}\mathcal{SI}_{-2}$		✓		0.0007	−0.0021
22	$\delta_{\text{swall}}\mathcal{SI}_{-1}$		✓		0.0003	−0.0018
23	$\delta_{\text{swall}}\mathcal{CTRL}$		✓		0.0	−0.0014
24	$\delta_{\text{swall}}\mathcal{SI}_{1}$		✓		−0.0004	−0.0011
25	$\delta_{\text{swall}}\mathcal{SI}_{2}$		✓		−0.0007	−0.0007
26	$\delta_{\text{wall}}\mathcal{SI}_{-2}$			✓	0.0007	−0.0021
27	$\delta_{\text{wall}}\mathcal{SI}_{-1}$			✓	0.0003	−0.0018
28	$\delta_{\text{wall}}\mathcal{CTRL}$			✓	0.0	−0.0014
29	$\delta_{\text{wall}}\mathcal{SI}_{1}$			✓	−0.0004	−0.0011
30	$\delta_{\text{wall}}\mathcal{SI}_{2}$			✓	−0.0007	−0.0007

Note. The naming of the experiments and their components can be understood as follows. δ_d indicates the bathymetry (d is the boundary condition), salt flux forcing $\mathcal{CTRL}/\mathcal{SI}_c/\mathcal{CST}_c$ used, c is the strength of the forcing (see below) and $\mathcal{CTRL}$ is the control freshwater flux. $\mathcal{SI}_*$ experiments modify the meridional gradient in salt flux (e.g., more/less sea ice) and $\mathcal{CST}_*$ is a uniform offset in the magnitude of salt flux. Control ($\mathcal{CTRL}$) experiments are repeated in the above table for readability (3, 8, 13 are the same as 18, 23, 28 respectively). δ_{NONE} refers to a re-entrant channel, δ_{swall} is a blocked shelf and δ_{wall} is a blocked shelf and deep open ocean. See Figure 2 for details.

freshwater in the north where it is melted. To calculate the annual flux, we use NASA sea ice data (Vaughan et al., 2013; "World of Change," 2009). To calculate the flux, assuming 0.5 m of sea ice, we calculate the approximate annual change of volume of sea ice 7.5×10^{12} m^3 and then divide by the area of the Southern Ocean and seconds in a year to get a freshwater flux of 1.1×10^{-5} kg m^{-2} s^{-1}. This is the average freshwater flux over the region of sea ice growth. For simplicity we assume a linear decrease in the freshwater flux associated with sea ice. Taking a value of 2×10^{-5} kg m^{-2} s^{-1} at the southern boundary of the domain and -2×10^{-5} kg m^{-2} s^{-1} at the northern boundary gives the desired result of an average of 1×10^{-5} kg m^{-2} s^{-1} freshwater taken out over the southern half, balanced by an average of -1×10^{-5} kg m^{-2} s^{-1} put in over the northern half. Adding this to the

constant freshwater flux from precipitation then gives a control simulation with mean flux of -2×10^{-5} kg m^{-2} s^{-1} and a range of 4×10^{-5} kg m^{-2} s^{-1}. Converting this into salt flux gives a mean flux of 7×10^{-4} g/m^{2}s and a range of 1.4×10^{-3} g/m^{2}s of salt, which is the basis of our control salt flux forcing.

Figure 1 shows the resulting forcings based on the above idealized forcing. We thus have 9 forcings based on a constant offset (Figure 1a) and a change in meridional freshwater flux gradient (Figure 1b). By design, the $\mathcal{CST}$ "constant" experiments do not change the meridional gradient in the forcing and the $\mathcal{SI}$ "sea ice" experiments do not have a change in their mean. $\mathcal{CST}_{-2}$, $\mathcal{CST}_{-1}$ (purple; Figure 1a) have a positive uniform change in salt flux, since the control forcing has zero salt flux at the southern boundary, the $\mathcal{CST}_{-2}$ and $\mathcal{CST}_{-1}$ perturbations result in regions where the freshwater flux becomes positive (i.e., injection of salt). Similarly, $\mathcal{CST}_1$, $\mathcal{CST}_2$ (green; Figure 1a) are uniform increases in the freshwater flux. Whereas the $\mathcal{SI}$ "sea ice" experiments are intended to emulate a change in the volume of total sea ice where such changes create a different redistribution of freshwater. $\mathcal{SI}_1$, $\mathcal{SI}_2$ (green; Figure 1b) are decreases in overall annual sea ice volume, where $\mathcal{SI}_1$ is the situation where there is no longer any sea ice. $\mathcal{SI}_{-2}$, $\mathcal{SI}_{-1}$ (purple; Figure 1b) can be thought of as an increase in sea ice; these two cases have a sign change in the salt flux at the southern boundary whereby salt is being added. Perturbation magnitude is similar to the realistic configuration projection based forcing seen in Figure 1a in (Shi et al., 2020).

The flow regimes and geometry of the Southern Ocean (Figure 2a) are emulated with three different bathymetries (Figures 2b–2g). All bathymetries have the same common sea floor, deep ocean ridge and shelf. The first case (δ_{NONE}) only consists of this sea floor, 900 m ridge and shelf, whereas cases 2–3 (δ_{swall} and δ_{wall}) have a wall at 405 km that is two grid cells wide. Since the western-eastern boundary is re-entrant, the construction of a wall is effectively changing the boundary condition. Thus, in the case of δ_{NONE} we are in a throughflow regime and in δ_{wall} a gyre regime. In the case of δ_{swall} there is a mix of flow regimes, namely a gyre regime on the shelf and a throughflow regime in the deep ocean. Whilst these geometries are very idealized, they can be considered relevant to different Antarctic regions (Figure 2a). For example, the Amundsen sea and Eastern Antarctica are like δ_{NONE} with unblocked throughflow both on the shelf and in the deep ocean. In contrast, the Weddell Sea has a wall to the west due to the Antarctic peninsula which makes it similar to the geometry of δ_{wall}. In some sense, the Ross Sea is similar, constrained by steep f/h contours to the west created by the Pacific-Antarctic ridge (Patmore, 2019). However, unlike the Weddell Sea, the very strong constraint of continental blocking only occurs on the shelf (Figure 2a); in another sense then, it is like the δ_{swall} case. In other regions, the geometry of the continent and bathymetry off the shelf are relevant to the δ_{swall} bathymetry. For example, Thurston Island, situated in between Bellingshausen and Amundsen seas blocks off a large part of the shelf in the Bellingshausen. Clearly, none of these examples is completely captured by the idealized set up used here but this approach does capture the range of responses that are possible in these extreme examples. Figure 3 gives visual context to the modeling setup used in this study for a single experiment, namely $\delta_{\text{wall}}\mathcal{CTRL}$. Figure 3 shows the main forcing elements: the surface freshwater forcing ("Salt Flux" layer) and the wall at 405 km, as well as the deep ocean ridge ("Bathymetry" layer). In the "Sea Surface Height" layer, we see imprints of the three gyres that are created from the δ_{wall} geometry, as well as their zonal flows ("Zonal velocity" layer). The temperature structure arising from these factors results in a warm shelf ("Temperature"). These details are re-visited in Section 3.1.

From Figures 1 and 2, taking all combinations of the 9 freshwater forcings (Figure 1; $\mathcal{CTRL}$, $\mathcal{CST}_{-2}$, $\mathcal{CST}_{-1}$, $\mathcal{CST}_1$, $\mathcal{CST}_2$, $\mathcal{SI}_{-2}$, $\mathcal{SI}_{-1}$, $\mathcal{SI}_1$, $\mathcal{SI}_2$) with three different bathymetries (Figure 2; δ_{NONE}, δ_{swall} and δ_{wall}) gives 27 experiments (Table 2).

All simulations in this paper have a spin-up of 90 years where the time-mean values of a further 10 years are used for all analysis.

3. Results

3.1. Summary of Mean State Circulation for Throughflow and Gyre Regimes

Figure 4 shows mean circulation diagnostics of the two "bookend" cases with a control freshwater forcing, namely, $\delta_{\text{NONE}}\mathcal{CTRL}$, which is in a throughflow regime, and $\delta_{\text{wall}}\mathcal{CTRL}$, which is in a gyre regime. Comparing Figures 4a and 4f the gyre case has warmer waters on the shelf compared to the throughflow regime case. Interestingly this is the opposite to what was found in B25 (Figure 6f B25) and is a result of the change in surface forcing from a restoring condition to a surface salt flux (the only difference between the two configurations). Here, the clockwise meridional overturning cell created by the westerly winds with δ_{wall} bathymetry is larger than

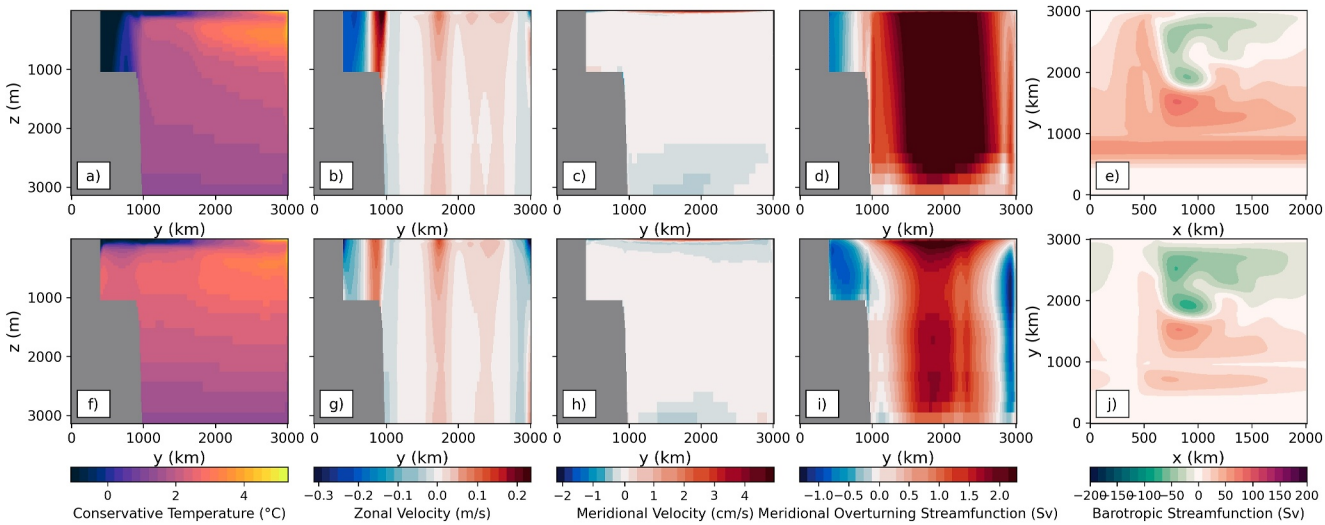

Figure 4. Overview of the mean state of the open (first row; δ_{NONE}) and closed channel (second row; δ_{wall}) with control freshwater forcing. Along the columns: Conservative Temperature (°C), Zonal Velocity (m/s), Meridional Velocity (cm/s), Meridional Overturning Streamfunction (*Sv*) and Barotropic Streamfunction (*Sv*) where the first three are the zonal average.

B25 (Figure 6j) with an extent that nears the shelf break, driving warm deep waters up the shelf. Additionally, B25 has a warmer shelf at depth in a throughflow regime and cooler above ∼700 m offshore (Figure 6a B25). The restoring profile used in B25 had only small changes in salinity (∼0.2 g/kg) whereas the salt flux forcing used here has a large meridional gradient where the absolute value goes to zero at the coast; these differences result in an upper ocean that is fresher and more stratified. Notably $\delta_{\mathrm{wall}}\mathcal{SI}_{-2}$ (Figure 6k) with a large addition of salt over the shelf, resembles B25 Figure 6f. In general, the large-scale circulation is consistent with what we would expect from linear theory. Considering the barotropic streamfunctions, the δ_{wall} bathymetry in Figure 4j blocks

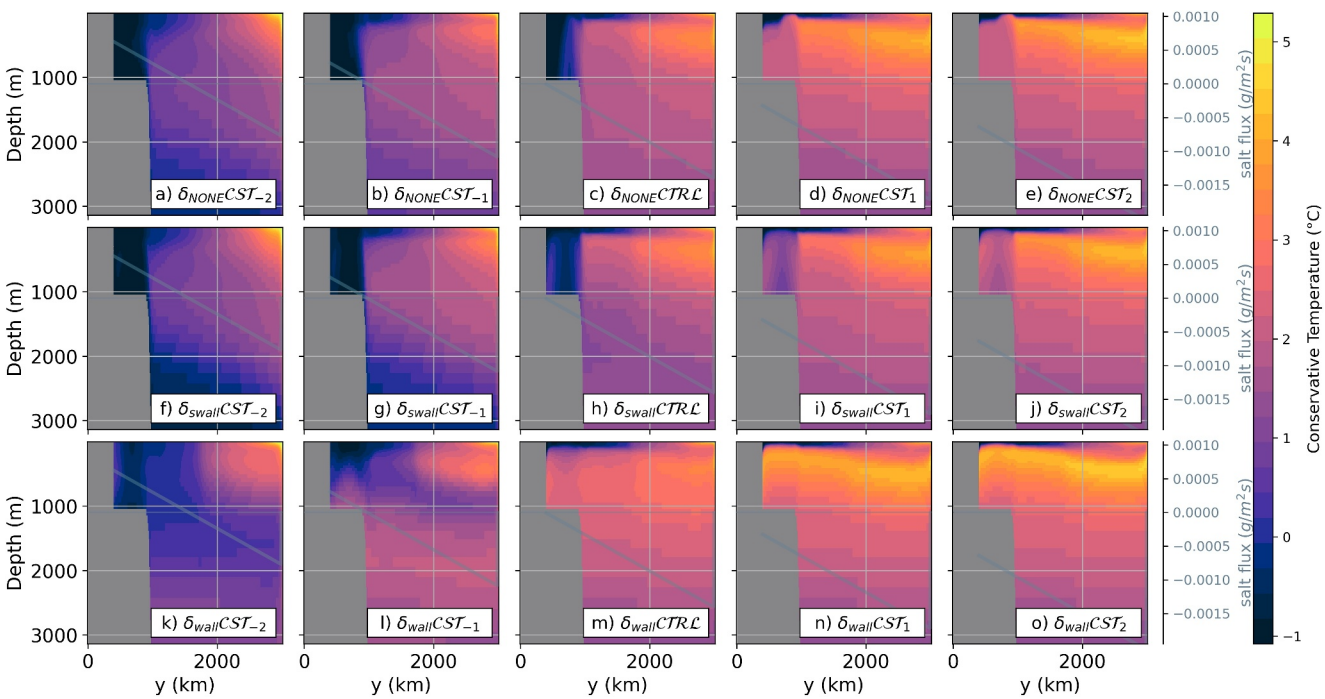

Figure 5. Zonal mean temperature for *uniform offset* experiments (1–15; Table 2). Each column has a new freshwater forcing (Figure 1a) where the middle column is the control experiment. The gray line highlights the zonally averaged freshwater. Each row has a different boundary condition, in order: (i) fully re-entrant, (ii) blocked shelf and (iii) fully blocked shelf and deep ocean, respectively. This panel-experiment layout also applies to Figures 6–8 and 11, 12.

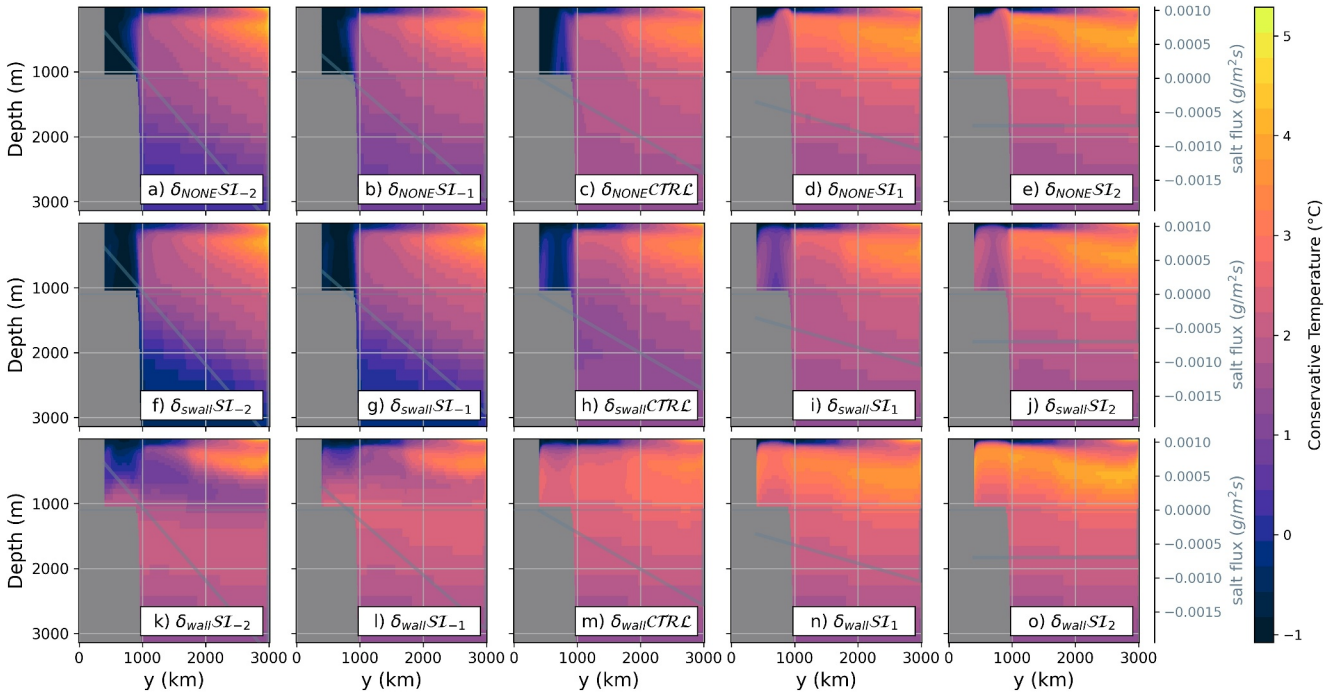

Figure 6. Same as previous figure but for zonal mean temperature for *sea ice* experiments (16–30; Table 2). Each column has a new freshwater forcing (Figure 1b) where the middle column is the control experiment. The gray line highlights the zonally averaged freshwater. Each row has a different boundary condition, in order: (i) fully re-entrant, (ii) blocked shelf and (iii) fully blocked shelf and deep ocean, respectively.

throughflow at $x = 405$ km creating barotropic gyres in the deep ocean and shelf. The addition of a continental shelf introduces steep f/h gradients, leading to an additional gyre in the south (same direction as the curl is unchanged over that region). In contrast, the absence of a wall at $x = 405$ km with bathymetry δ_{NONE} in Figure 4e, permits baroclinic flow in the deep ocean and leads to a throughflow on the shelf. The zonal averages in zonal velocity, meridional velocity and overturning (Figures 4b–4d, 4g–4i) are consistent with these large-scale flow features.

3.2. Shelf Temperatures Resulting From Changes in Surface Salt Flux and Circulation Regime

This section documents how shelf temperatures are modulated by the surface salt flux and change in flow regime. Figures 5 and 6 communicate the main results of this study, they show large changes in shelf temperatures from both: a uniform offset (Figure 5; $\mathcal{CST}_*$) and change in the meridional gradient in salt flux (Figure 6; $\mathcal{SI}_*$). Zonal mean temperature differences (same data as Figures 5 and 6) with control experiment removed are shown in Figures S2 and S3 in Supporting Information S1. Figures 7 and 8 shows an $x - z$ slice of temperature along the imagined ice front (indicated Figure 2b).

Figure 5 shows that negative uniform shifts in the salt flux (e.g., uniform increases in precipitation) have a dramatic influence on warm waters getting onto the shelf. Across all flow regimes (bathymetries), simulations ($\delta_*\mathcal{CST}_1$; $\delta_*\mathcal{CST}_2$; Figures 5 and 7 columns 3–4) with the strongest freshening (removal of salt) have a warm shelf as a result of the applied surface forcing changes. We can now revisit the open question posed in Section 1: "Can changes in cross-slope freshwater gradients or changes in the total amount of precipitation significantly affect shelf temperatures?" The sea ice experiments in which there is less sea ice, that is, the south-north salinity gradient is flattened ($\delta_*\mathcal{SI}_1$; $\delta_*\mathcal{SI}_2$; Figures 6 and 8 columns 3–4) also result in a warm shelf. So in terms of shelf temperatures, this suggests that a uniform change or gradient change in the salt flux can *both* effectively drive warmer waters onto the shelf. In the case where there is an increase in salt flux forcing and some part of the domain is unblocked ($\delta_{\text{NONE}}, \delta_{\text{swall}}$ with $\mathcal{CST}_{-2}, \mathcal{CST}_{-1}, \mathcal{SI}_{-2}, \mathcal{SI}_{-1}$; Figures 5 and 6a, 6b, 6f, 6g) the shelf near the ice front is cold and in these instances there is a positive salt flux in the shelf region where deep convection is occurring (see zero crossing gray line Figures 5 and 6), discussed in more detail in Section 3.3.

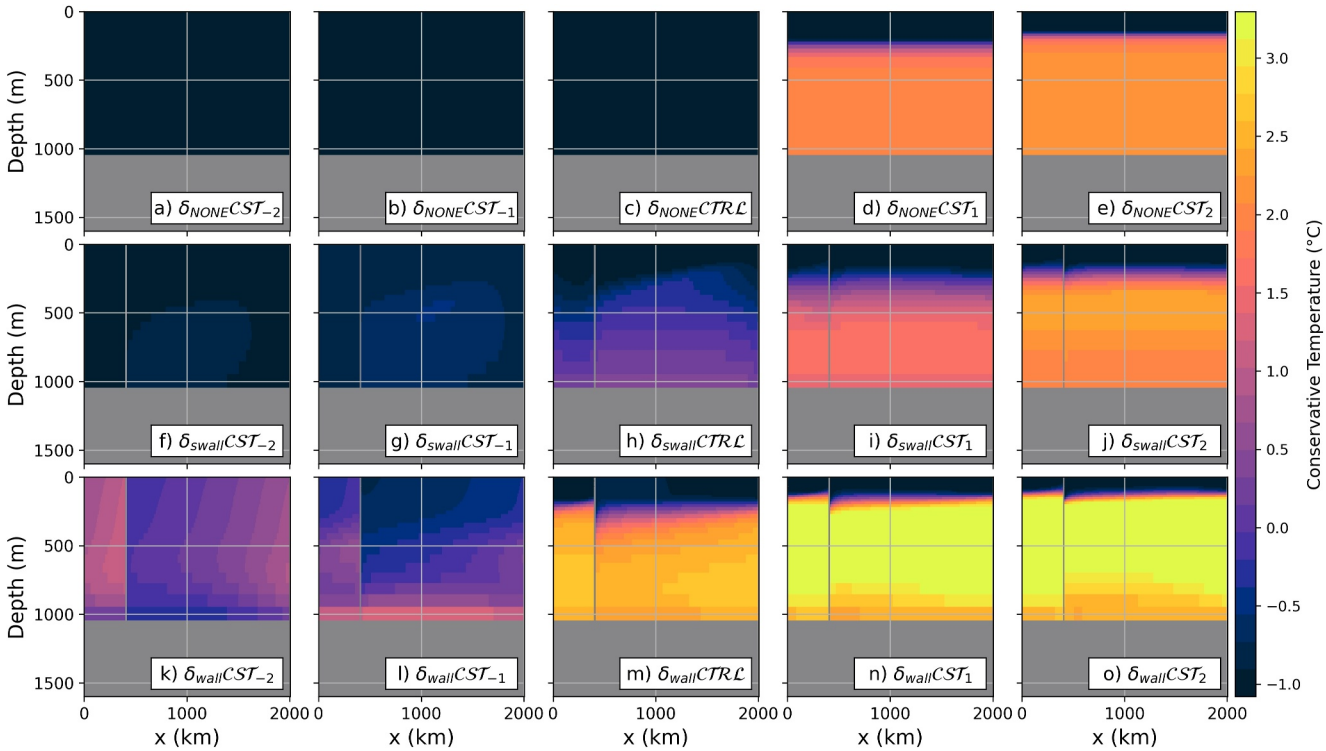

Figure 7. Same panel-experiment layout as Figure 5 but for southern boundary ("ice front" indicated Figure 2b) mean temperature and *uniform offset* experiments. Each row has a different boundary condition, in order: (i) fully re-entrant, (ii) blocked shelf and (iii) fully blocked shelf and deep ocean, respectively. Note there is a wall at $x = 405$ km on the shelf in δ_{swall} and δ_{wall}.

Across both the forcing cases and warming simulations ($\delta_*\mathcal{CST}_1$, $\delta_*\mathcal{CST}_2$ and $\delta_*\mathcal{SI}_1$, $\delta_*\mathcal{SI}_2$; Figures 5 and 6, respectively, columns 3–4), the warmer waters are predominantly entering the shelf from the northern boundary restoring the region at ~500 m (Figures S2 and S3 in Supporting Information S1). However, in some cases there is greater warming at depth in the open ocean, for example, comparing $\delta_{\text{swall}}\mathcal{CST}_2$, $\delta_{\text{wall}}\mathcal{CST}_2$, $\delta_{\text{swall}}\mathcal{SI}_2$, $\delta_{\text{wall}}\mathcal{SI}_2$ (Figures S2, S3j, and S3o in Supporting Information S1). Interestingly, the warming and cooling patterns occur at different depths (comparing columns 1–2 and 3–4 in Figures 5, 6, and S2, S3 in Supporting Information S1) with cooling happening more at depth than warming (mostly above 2,000 m), this is likely due to increases in freshwater increasing stratification and trapping fresher waters near the surface. In contrast, with buoyancy loss at the surface, shelf waters are able to mix vertically via the creation of denser waters that are then able to sink and flow off the shelf. This relatively dense water can then enter the open ocean deeper in the water column and extend the depth range of the temperature anomaly. A further application of this idea is also related to the asymmetric temperatures changes, namely, the deep offshore cooling being strongest when the shelf is in a gyre regime ($\delta_{\text{swall}}\mathcal{CST}_{-2}$; Figures 5 and S2f, S6f in Supporting Information S1), possibly driven by the change in the wind driven northward return flow on the shelf, with the introduction of a wall. Recall that the easterlies on a flat bottomed shelf and open boundary lead to cold surface waters that downwell at the southern boundary and will be confined to a return flow on the bottom Ekman layer (Olbers et al., 2012). When a wall is introduced, the return flow becomes a northward geostrophic flow that is distributed over the height of the wall. This can enhance mixing with shelf waters creating further dense water that can then flow off the shelf. The influence of boundary conditions is discussed next and stratification changes are discussed in more detail in Section 3.3.

Within both kinds of forcings ($\mathcal{CST}_*$ and $\mathcal{SI}_*$), the flow regime (bathymetry) influences the amount to which the same perturbation can modify shelf temperatures. Looking across row 3 in Figures 5–8, experiments $\delta_{\text{wall}}\mathcal{CST}_*$ and $\delta_{\text{wall}}\mathcal{SI}_*$ show a gradual warming as the freshwater forcing changes in the fully blocked case. This insensitivity to flow regime (boundary condition) is in contrast to B25, where uniform constant wind changes were found to have a strong sensitivity in δ_{NONE}, δ_{swall} cases but limited sensitivity in δ_{wall} (Figures 7 and 8 in B25). Also across both types of forcings ($\mathcal{CST}_*$ and $\mathcal{SI}_*$) and like B25, the flow regime influences the amount of warm

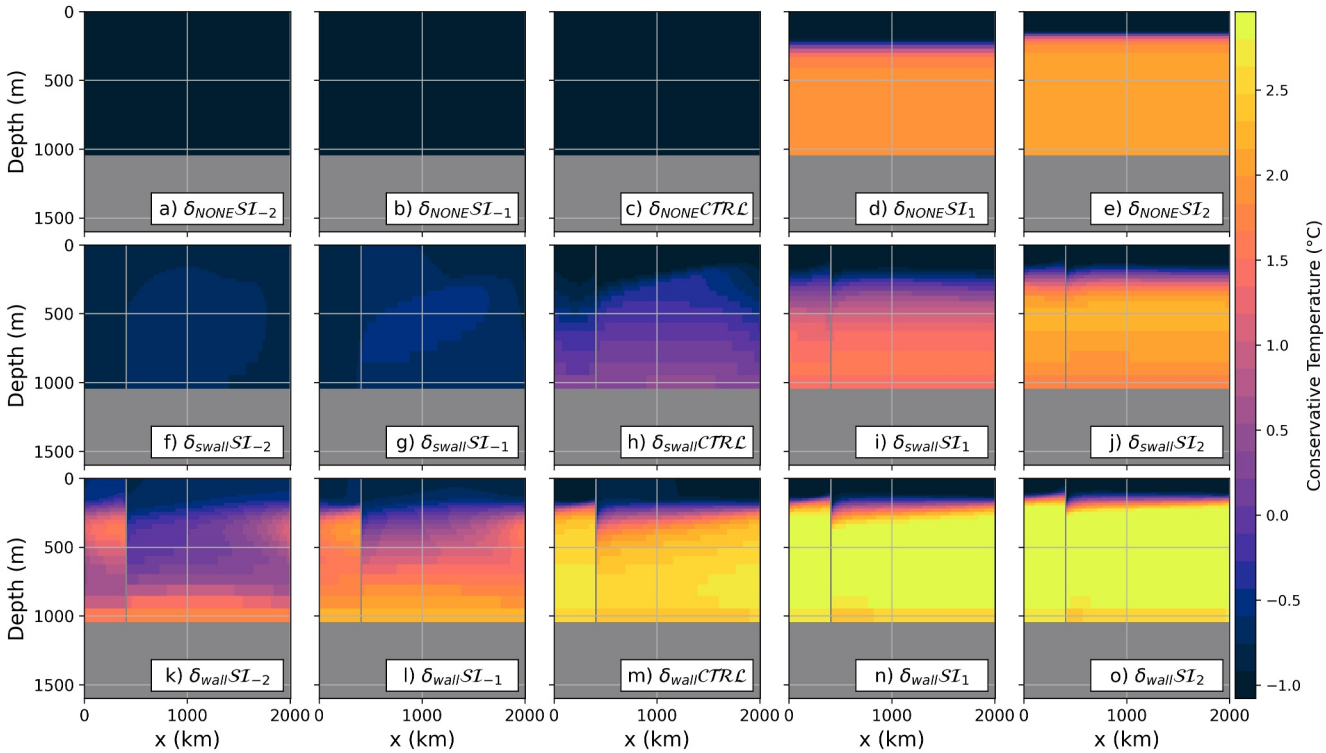

Figure 8. Same panel-experiment layout as Figure 4 but for southern boundary ("ice front" indicated Figure 2b) mean temperature and *sea ice* experiments. Each row has a different boundary condition, in order: (i) fully re-entrant, (ii) blocked shelf and (iii) fully blocked shelf and deep ocean, respectively. Note there is a wall at $x = 405$ km on the shelf in δ_{swall} and δ_{wall}.

water that ends up on the shelf under the same perturbation ($\delta_*\mathcal{CTRL}$; middle column Figure 5). Given the similarity between the response of $\delta_*\mathcal{CST}_*$ and $\delta_*\mathcal{SI}_*$ experiment sets, the remainder of this paper will focus on the uniform constant offset experiments ($\delta_*\mathcal{CST}_*$). Supporting information also shows results for $\delta_*\mathcal{SI}_*$ where appropriate (Figures S3, S5, S7, S9, S13, S14 in Supporting Information S1).

3.3. Large-Scale Changes in Density, Salinity and Temperature From Salt Flux Forcing Changes and Circulation Regime

The changes in zonally averaged temperature shown in Figures 5 and 7, can be further understood in terms of the changes in prescribed freshwater flux and their influence on the stratification (dominated by salinity in the Southern Ocean). This final results section focuses on the uniform offset experiments. Here, we quantify the water mass changes in terms of 3 key regions (Figure 9) and then characterize the large-scale stratification changes that lead to the described shelf temperature changes (Figures 10–13).

Figure 9 shows a quantitative regional summary of the changes in temperature, salinity and density at the "ice front," "shelf" and "offshore" regions (pictured in Figure 2b). The temperature, salinity and density of the $\mathcal{CTRL}$ simulations is most similar between δ_{NONE}, δ_{swall} where δ_{wall} is typically more different than the other two (Figure 9), the large-scale reasons for this will be explored in more detail below. Across all regions and simulations, warming occurs when a constant offset to the freshwater forcing is added (across $\mathcal{CST}_{-2}, \mathcal{CST}_{-1}, \mathcal{CTRL}, \mathcal{CST}_1, \mathcal{CST}_2$ in Figures 9a, 9d, and 9g). Relatedly, as the freshwater flux increases, all regions experience a decrease in salinity and density (across $\mathcal{CST}_{-2}, \mathcal{CST}_{-1}, \mathcal{CTRL}, \mathcal{CST}_1, \mathcal{CST}_2$ in Figures 9b, 9c, 9e, 9f, 9h, and 9i) with the largest changes occurring between $\mathcal{CST}_{-2}, \mathcal{CST}_{-1}$ and $\mathcal{CTRL}$. As described in Section 3.2 (Figures 5 and 7), a positive uniform offset in the forcing leads to a non-linear warming in temperature in the "ice front" region across all flow regimes (Figure 9a). The biggest change in warming (2.7°C) is between $\delta_{\text{NONE}}\mathcal{CTRL}$ and $\delta_{\text{NONE}}\mathcal{CST}_1$ (green triangle; Figure 9a), this is also true for the sea ice experiments (Figure S14a in Supporting Information S1). A large change in "ice front" temperature (1.8°C) also occurs between $\delta_{\text{wall}}\mathcal{CST}_{-1}$ and $\delta_{\text{wall}}\mathcal{CTRL}$ (orange diamond; Figure 9a).

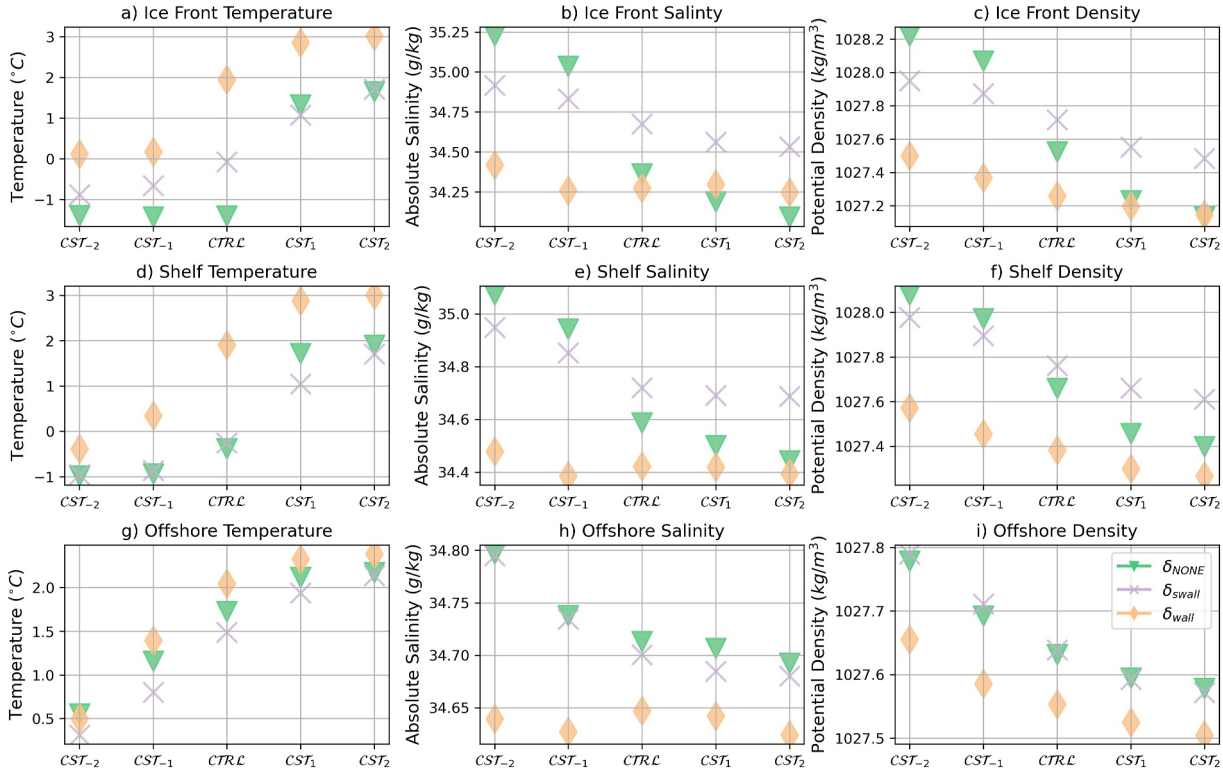

Figure 9. Region averaged temperature (column 1), salinity (column 2) and density (column 3) for *uniform offset* experiments. Each boundary condition (δ_{NONE}; δ_{swall}; δ_{wall}) is described by a different marker in legend in panel i. Regions are "ice front" (row 1), "shelf" (row 2) and "offshore" (row 3) and pictured in Figure 2b.

Comparing the $\mathcal{CTRL}$ simulation's meridional profile of depth and zonally averaged density in Figures 10a–10c (black lines). The shape and gradients of density look similar when the deep ocean is in a throughflow regime (the bathymetry has an unblocked deep ocean in $\delta_{\text{NONE}}\mathcal{CTRL}$; $\delta_{\text{swall}}\mathcal{CTRL}$; Figures 10a and 10b). There is also much higher density on the shelf when in a gyre regime on the shelf and deep ocean ($\delta_{\text{wall}}\mathcal{CTRL}$; Figure 10c). This is consistent with the deep ocean's stratification being largely set by the flow regime. Focusing separately on each subplot in Figure 10 (i.e., keeping the bathymetry constant), we see that meridionally constant offsets in the zonally averaged salt flux lead to large-scale near uniform offsets in density across all bathymetries. Specifically, we have lighter waters under freshening forcing ($\delta_*\mathcal{CST}_1$; $\delta_*\mathcal{CST}_2$) and denser waters under salinifying forcing ($\delta_*\mathcal{CST}_{-1}$; $\delta_*\mathcal{CST}_{-2}$). Figure 10 also shows how the flow regime influences the magnitude of density change on the shelf with a change in forcing. In general, the change in density on the shelf at the southern boundary is much larger when the shelf is unblocked (e.g., comparing $\delta_{\text{NONE}}\mathcal{CST}_1$; $\delta_{\text{swall}}\mathcal{CST}_1$; Figures 10a and 10b) and results in a relatively strong meridional density gradient over the shelf. This could explain how the $\delta_{\text{NONE}}\mathcal{CST}_1$ simulation (Figure 7d) shows the largest increase in temperature at the southern boundary coming from the $\delta_{\text{NONE}}\mathcal{CTRL}$ simulation (Figure 7c), as compared to the weaker relative warming in the blocked cases ($\delta_{\text{swall}}\mathcal{CTRL}$; $\delta_{\text{swall}}\mathcal{CST}_1$; $\delta_{\text{wall}}\mathcal{CTRL}$; $\delta_{\text{wall}}\mathcal{CST}_1$; Figures 7h, 7i, 7m, and 7n). We will re-visit the cause of this larger shelf density gradient below.

Figure 11 highlights how the upper ocean's zonally averaged potential density changes with a change in surface forcing and flow regime. Figure 11 allows us to connect how the meridional density gradient changes discussed in Figure 10 influences stratification at depth and shelf temperatures (Figure 5). Figure 11 and Figure S4 in Supporting Information S1 (showing anomalies from the control), highlight stratification changes that are consistent with the temperature changes described in Section 3.2. The sea ice experiments also have similar changes in zonally averaged salinity and density in Figure S5 in Supporting Information S1. Fixing the salt flux by looking down the columns in Figure 11, we can see that the advection of salt by the mean circulation creates a large-scale reorganization of the same salt flux resulting in an inflation of some isopycnals and change in the zonally averaged gradient in others. A fresher forcing leads to lighter waters in the now more strongly stratified upper layers ($\delta_*\mathcal{CST}_1$; $\delta_*\mathcal{CST}_2$; Figure 11, S6 columns 3 or 4 in Supporting Information S1), and conversely, adding salt

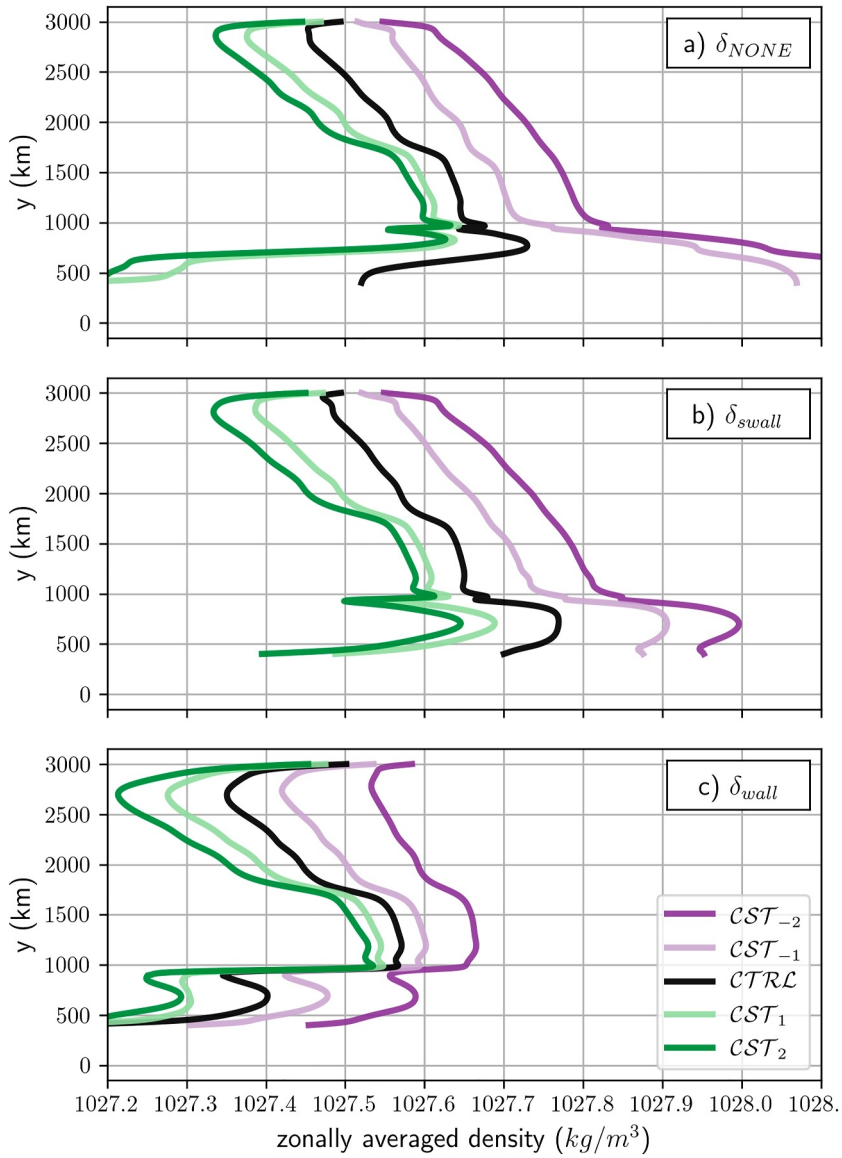

Figure 10. Depth and zonal mean average density for *uniform offset* experiments ($\mathcal{CST}_{-2}$, $\mathcal{CST}_{-1}$, $\mathcal{CTRL}$, $\mathcal{CST}_{1}$, $\mathcal{CST}_{2}$ purples, black, greens, as Figure 1a) where each row has a different boundary condition ($\delta_{\text{NONE}}, \delta_{\text{swall}}, \delta_{\text{wall}}$).

leads to a very dense shelf in most cases triggering deep convection of cool surface waters (e.g., $\delta_{\text{NONE}}\mathcal{CST}_{-2}$; $\delta_{\text{swall}}\mathcal{CST}_{-2}$; Figures 5a, 5f and 11a, 11f). Consistent with Figure 10, in the case of a throughflow regime on the shelf (top row Figure 11), the near surface southern boundary density changes a lot with the change in surface forcing. In particular, a freshening perturbation ($\delta_{\text{NONE}}\mathcal{CST}_{1}$; $\delta_{\text{NONE}}\mathcal{CST}_{2}$; Figures 11d and 11e) increases stratification on the shelf. This surface freshening from the forcing increases stratification, blocking the downwelling of cool surface waters near the southern boundary. As the new isopcynals slope more steeply upwards toward the shelf (Figure 11 and S6 in Supporting Information S1) warmer waters are able to flow across isopcynals toward the southern boundary. When salt is added (e.g., $\delta_{\text{NONE}}\mathcal{CST}_{-2}$; Figure 11a), the near-surface becomes denser, driving vertical mixing and reducing southward isopcynal heat transport of warm waters, leading to a cooler shelf where increased salt release near the southern boundary drives convection of cool surface waters. Comparing Figures 5 and 11, we can see that the changes in slope, structure and thickness of the isopcynals have a direct influence on the temperature on the shelf. Consistent with previous studies (Caillet et al., 2023; Daae et al., 2020; Haid et al., 2023), Figure 11 shows that there is a cross-slope density gradient threshold which leads to warm shelf temperatures. The 1,027 kg m^{-3} isopcynal (red Figures 11 and S4 in

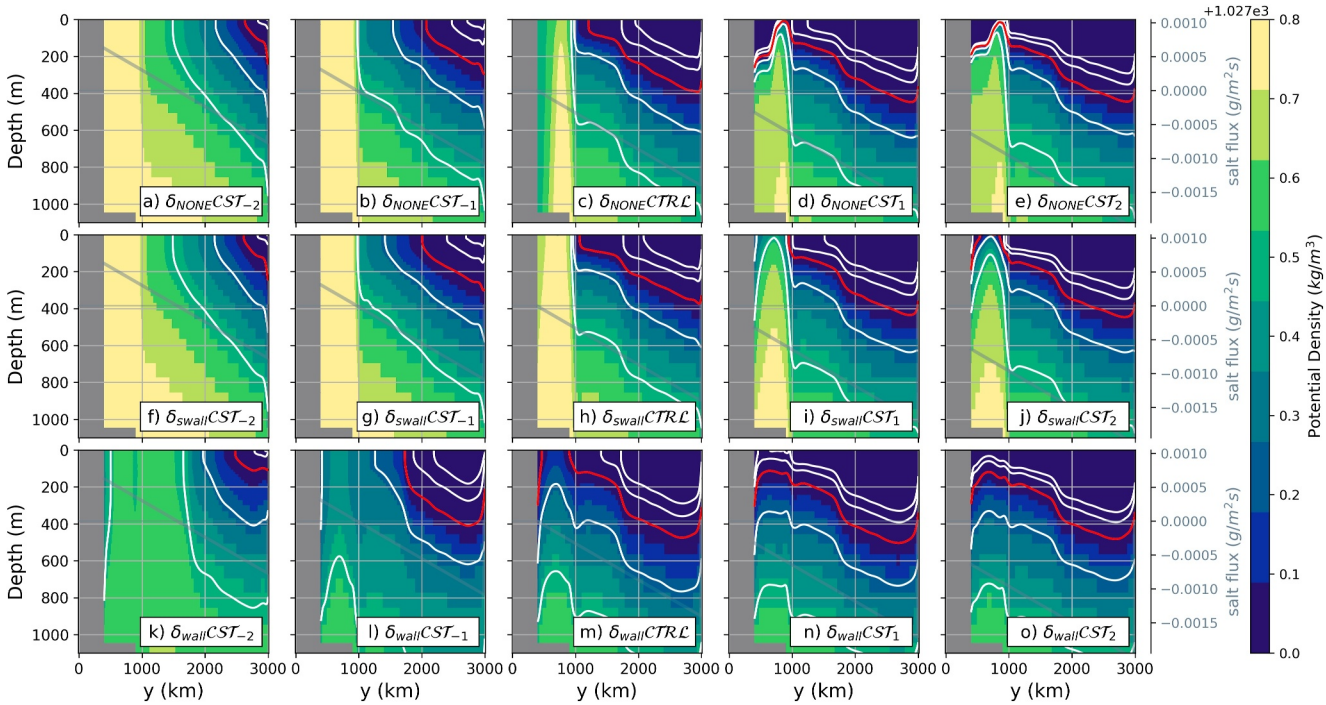

Figure 11. Zonal mean potential density for *constant uniform offset* experiments for the upper 1,100 m. Solid contours: 1026.5, 1026.75, 1027, 1027.25, 1027.5 isopcynals; all are white except for 1,027 which is red. Each column has a new freshwater forcing where the middle column is the control freshwater. The gray line shows the freshwater forcing.

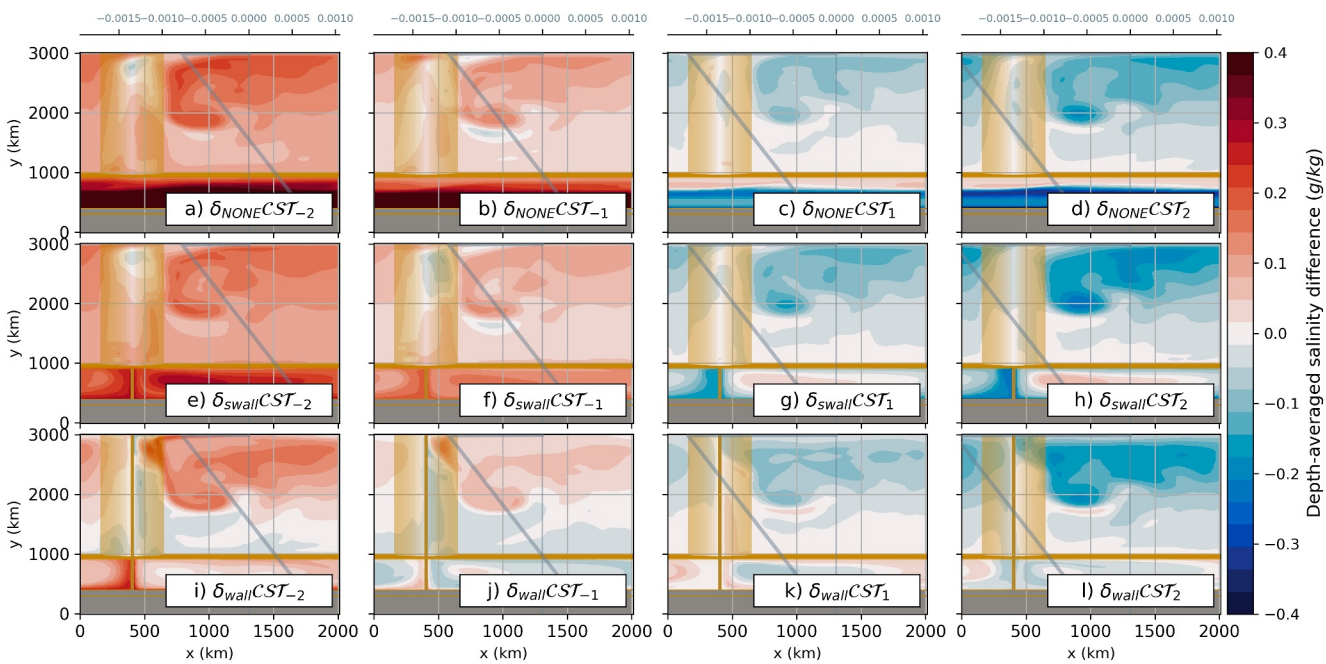

Figure 12. Depth averaged salinity difference for *uniform offset* experiments with control experiment removed (control being relative to boundary condition). Gray lines shows salt flux forcing and tan lines show bathymetry. Each row has a different boundary condition, in order: (i) fully re-entrant, (ii) blocked shelf and (iii) fully blocked shelf and deep ocean, respectively. Raw values are shown in Figure S8 in Supporting Information S1.

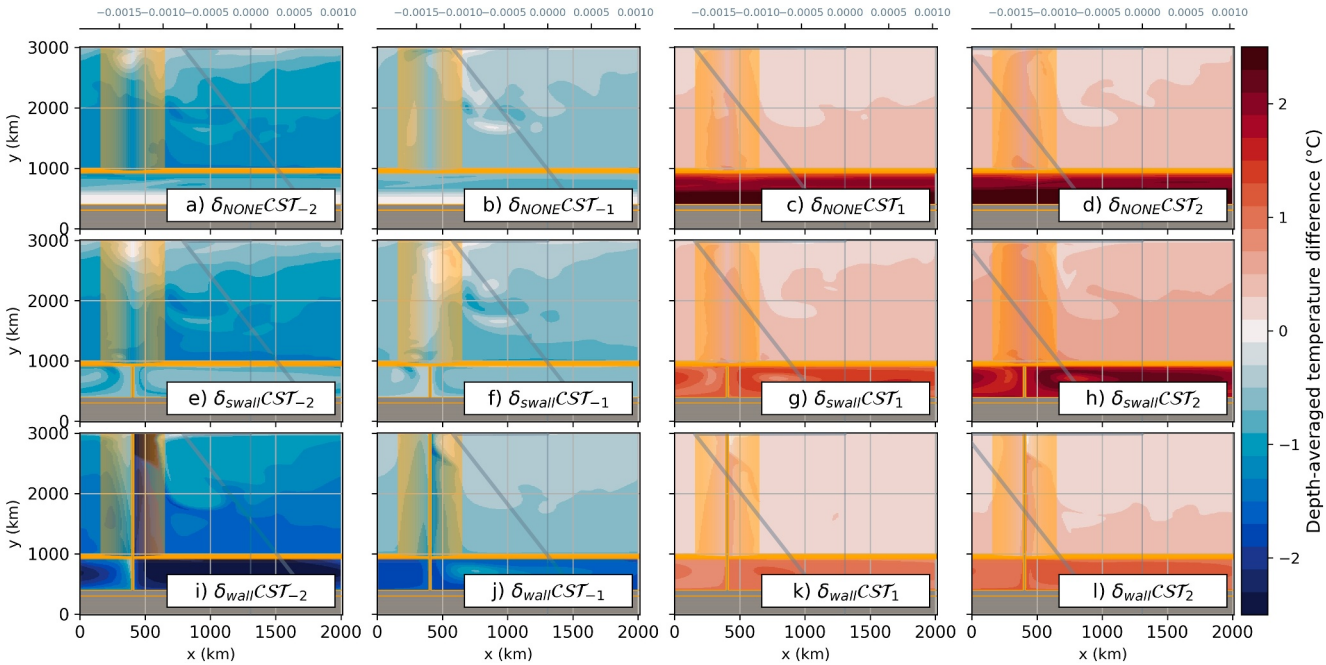

Figure 13. Depth averaged temperature difference, for *uniform offset* experiments with control experiment removed (control being relative to boundary condition). Gray lines shows salt flux forcing and cyan lines show bathymetry. Each row has a different boundary condition, in order: (i) fully re-entrant, (ii) blocked shelf and (iii) fully blocked shelf and deep ocean, respectively.

Supporting Information S1) is the key indicator of whether the shelf has substantial warm water on it. Applying this idea, it is possible to separate all experiments into ones in which the 1,027 kg m^{-3} isopycnal intersects the southern boundary leading to a warm ice front (Figures 5, 7, and 11d, 11e, 11j, 11m–11o) and in the case where the isopcynal outcrops at the surface, the ice front is relatively cold (Figures 5 and 7a–7c, 7f, 7g, 7h, 7k, 7l). This partition works everywhere except for $\delta_{\text{swall}}\mathcal{CST}_1$ (Figures 7i and 11i).

Whilst the overall tendency is for the shelf to warm under a uniform decrease in the salt flux (Figure 5), the magnitude and spatial pattern of response is determined by bathymetry, via the circulation and flow regime. Figure 12 illustrates indirectly how the barotropic circulation (Figure S11 in Supporting Information S1) influences the depth averaged salinity and its response to a change in forcing. In key regions, we see imprints of the circulation regime in the patterns of salt flux *change*. Fixing the salt flux, in Figures 12c, 12g, and 12k, we can see that the resulting strong freshening on the shelf in the cases when the shelf is unblocked ($\delta_{\text{NONE}}\mathcal{CST}_1$ in Figure 12c), is relatively strong ($\delta_{\text{swall}}\mathcal{CST}_1$; Figure 12g) because it is zonally uniform due to being in a throughflow regime. This also explains why when observing heat changes at the ice front ($\delta_{\text{NONE}}\mathcal{CST}_1$; Figure 7d), the temperature changes are also zonally uniform (Figure S12 in Supporting Information S1). In contrast, the blocked shelf cases (gyre regime on the shelf) have weaker gradients on the shelf due to cancellation between positive/negative changes in density ($\delta_{\text{swall}}\mathcal{CST}_1$; $\delta_{\text{wall}}\mathcal{CST}_1$; Figures 11i and 11n) and a more domed temperature structure that is expected from a gyre on the shelf (Figures S11i and S11n in Supporting Information S1). Figure S12 in Supporting Information S1 clearly shows these features by taking a zonal temperature and salinity slice on the shelf (indicated in Figure 2g).

Figure 13 shows how the described changes in large-scale salinity lead to the described changes in shelf and ice front temperature in Figures 5 and 7. Overall, the circulation features discussed in terms of Figure 12 are also visible in Figure 13. Specifically, the circulation on the shelf influences the intensity and spatial structure of temperature on the shelf, being in a throughflow regime $\delta_{\text{NONE}}\mathcal{CST}_*$ (Figure 13 row 1) isotherms are zonally uniform, whereas the gyre on the shelf leads to $\delta_{\text{swall}}\mathcal{CST}_*$, $\delta_{\text{wall}}\mathcal{CST}_*$ (Figure 13 rows 2,3) domed isotherms (Figure 7 rows 2, 3). Additionally, as a uniform increase in freshening is applied (left to right along the columns of Figure 13), the whole domain warms where the zonal variation is explained by the mean circulation. In the zonally averaged sense, the warming mechanism can be summarized as follows. As the surface freshens, it shuts down vertical exchange processes on the shelf. That opens up the shelf to the intrusion of warm/salty water across the

shelf break, which was previously kept offshore by the creation of dense water on the shelf. The dense water ordinarily acts as a barrier, and when more of it is created, it can flow down the slope into the deep ocean.

4. Summary and Discussion

In this study, we have explored how large-scale basin geometry and large-scale changes in freshwater forcing at the surface, can play a role in determining the temperature structure on Antarctica's shelf seas. We used a primitive equation ocean model NEMO with varying flow regimes (bathymetry modifications that change the boundary conditions) and surface salt flux (Section 2), to test if changing the salt flux could draw warmer waters onto the shelf toward an imagined ice front at the southern boundary. Using 27 simulations, we tested two kinds of perturbations of the salt flux to emulate uniform changes in precipitation or sea ice. Spatially uniform changes in precipitation were emulated with a uniform constant offset of the salt flux, whereas changes in annual sea ice were emulated with a change in the meridional gradient of the salt flux. We were interested in exploring the possibility of a wind analogue to B25, namely, do gyre and throughflow regimes respond in the same way as winds in terms of constant offsets versus changes in meridional gradients in forcing. We sought the answer to two questions:

1. Can changes in cross-slope freshwater gradients or changes in the total amount of precipitation significantly affect shelf temperatures?
2. Like B25, is basin geometry important for modulating shelf temperature changes with freshwater changes?

This study has found, across all flow regimes (bathymetries), both a positive uniform increase or decrease in the meridional gradient of freshwater fluxes leads to warmer waters on the shelf. From the above discussion, we can now say "yes" to the above questions. Ultimately, we found that the mean circulation creates a large-scale reorganization of the same salt flux resulting in an inflation of some isopycnals and change in the zonally averaged gradient in others. An analysis of density and temperature on the shelf shows that when the 1,027 kg m^{-3} isopcynal intersects the southern boundary at depth, then the ice front is warm whereas in the cases when the same isopcynal outcrops at the surface, the shelf is relatively cold. Freshening from the forcing increases stratification, blocking the downwelling of cool surface waters near the southern boundary and provides greater buoyancy to the warmest waters, as the new isopcynals slope more steeply upwards toward the shelf, these waters are able to flow across isopcynals toward the southern boundary.

We also found that the flow regime (bathymetry) influences how susceptible the shelf is to changes in salt flux driving heat onto the shelf. The applied freshening flux is advected by the mean circulation, creating a large-scale reorganization of density enabling warmer waters to flow onto the shelf. On the large-scale, imprints of the circulation regime can be seen in the patterns of salt flux change, leading to different spatial patterns/magnitudes of warming under the same change in salt flux forcing. Whilst the overall tendency is for the shelf to warm under a uniform decrease in the salt flux, simulations with an unblocked shelf (throughflow regime on shelf) have the greatest change in warming with a decrease (more precipitaion) or reduced gradient (less sea ice) of the salt flux forcing. In these cases, compared to blocked shelf simulations (gyre regime on shelf), there is an increase in the meridional density gradient on the shelf from the existence of zonal flows, which leads to the described enhanced warming.

When it comes to understanding future Southern Ocean projections, we hope this and B25, demonstrate that the response of the system to both wind and freshwater changes needs to be considered carefully, as both changes in forcing can lead to dramatic changes in shelf temperatures through different mechanisms. A recent study by Shi et al. (2020) suggests that buoyancy forcing changes could be more important than winds in determining the Southern Ocean's temperature, and that changes in both lead to compensating effects in salinity. Here, the freshwater forcing was idealized to allow for the desired experimental design, we unrealistically chose to use a linear profile in sea ice related freshwater fluxes and presume that the precipitation in the Southern Ocean is a constant. A remaining question is in what sense are the extreme idealized freshwater forcings used here relatable to projected changes in the forcing of the Southern Ocean. An extreme projection done by Mathiot and Jourdain (2023) found that all sea ice could be gone by 2,300 under SSP5-8.5, Bracegirdle et al. (2020) found that by the end of this century under SSP5-8.5, the Southern Ocean could have a 31% increase in precipitation. The simulations conducted here then, more than span the range of projections over the coming centuries. An interesting follow up study could look at interactions between freshwater and wind changes, with a process focus.

Data Availability Statement

Key NEMO configuration files are available at https://doi.org/10.5281/zenodo.15627516. The NEMO configuration used in this article uses NEMO version 4.0.4 with the following branch: branches/UKMO/NEMO_4.0.4_momentum_trends @ 15194. This branch can be found on the (old svn) repository at: https://forge.ipsl.jussieu.fr/nemo/browser/NEMO/.

Acknowledgments
This work used the ARCHER2 UK National Supercomputing Service (https://www.archer2.ac.uk). C. B. and A. J. were supported by the European Union's Horizon 2020 research and innovation programme under grant agreement no. 820575 (TiPACCs). We thank three anonymous reviewers and Anna Wåhlin (editor) whose comments led to improvements in this manuscript.

References

Abernathey, R., Marshall, J., & Ferreira, D. (2011). The dependence of Southern Ocean meridional overturning on wind stress. *Journal of Physical Oceanography*, *41*(12), 2261–2278. https://doi.org/10.1175/JPO-D-11-023.1

Allison, L., Johnson, H., & Marshall, D. (2011). Spin-up and adjustment of the Antarctic Circumpolar Current and global pycnocline. *Journal of Marine Research*, *69*(2), 167–189. https://doi.org/10.1357/002224011798765330

Babu, N., Kumar, V., Sree Brahmanandam, P., Rao, M., Mekalathur, R. R., & Sreedhar, K. (2018). Anomalous wind circulation over Taipei, Taiwan during the northern winter seasons of 2004 and 2005- A case study. *Satellite Oceanography and Meteorology*, *3*(2). https://doi.org/10.18063/som.v3i2.666

Bernard, B., Madec, G., Penduff, T., Molines, J.-M., Treguier, A.-M., Le Sommer, J., et al. (2006). Impact of partial steps and momentum advection schemes in a global ocean circulation model at eddy-permitting resolution. *Ocean Dynamics*, *56*(5–6), 543–567. https://doi.org/10.1007/s10236-006-0082-1

Bhagtani, D., Hogg, A. M., Holmes, R. M., & Constantinou, N. C. (2023). Surface heating steers planetary-scale ocean circulation. *arXiv*. https://doi.org/10.48550/arXiv.2301.11474

Boyer, T. P., García, H. E., Locarnini, R. A., Zweng, M. M., Mishonov, A. V., Reagan, J. R., et al. (2018). World Ocean Atlas 2018 [Dataset]. *NOAA National Centers for Environmental Information*. https://www.ncei.noaa.gov/access/metadata/landing-page/bin/iso?id=gov.noaa.nodc:NCEI-WOA18

Bracegirdle, T. J., Krinner, G., Tonelli, M., Haumann, F. A., Naughten, K. A., Rackow, T., et al. (2020). Twenty first century changes in Antarctic and Southern Ocean surface climate in CMIP6. *Atmospheric Science Letters*, *21*(9), e984. https://doi.org/10.1002/asl.984

Bull, C. Y. S., Jenkins, A., Jourdain, N. C., Vaňková, I., Holland, P. R., Mathiot, P., et al. (2021). Remote control of Filchner-Ronne ice shelf melt rates by the Antarctic slope current. *Journal of Geophysical Research: Oceans*, *126*(2). https://doi.org/10.1029/2020JC016550

Bull, C. Y. S., Munday, D. R., & Jenkins, A. (2025). Influence of topography and winds on the distribution of water masses on the Antarctic Continental Shelf. *Journal of Physical Oceanography*, *55*, 1451–1473. https://doi.org/10.1175/JPO-D-24-0092.1

Cai, W., Gao, L., Luo, Y., Li, X., Zheng, X., Zhang, X., et al. (2023). Southern Ocean warming and its climatic impacts. *Science Bulletin*, *68*(9), 946–960. https://doi.org/10.1016/j.scib.2023.03.049

Caillet, J., Jourdain, N. C., Mathiot, P., Hellmer, H. H., & Mouginot, J. (2023). Drivers and reversibility of Abrupt Ocean State transitions in the Amundsen Sea, Antarctica. *Journal of Geophysical Research: Oceans*, *128*(1), e2022JC018929. https://doi.org/10.1029/2022JC018929

Colin de Verdière, A. (1989). On the interaction of wind and buoyancy driven gyres. *Journal of Marine Research*, *47*(3), 595–633. https://doi.org/10.1357/002224089785076172

Daae, K., Hattermann, T., Darelius, E., Mueller, R. D., Naughten, K. A., Timmermann, R., & Hellmer, H. H. (2020). Necessary conditions for warm inflow toward the Filchner Ice Shelf, Weddell Sea. *Geophysical Research Letters*, *47*(22). https://doi.org/10.1029/2020GL089237

Durack, P. J., & Wijffels, S. E. (2010). Fifty-year trends in Global Ocean salinities and their relationship to broad-scale warming. *Journal of Climate*, *23*(16), 4342–4362. https://doi.org/10.1175/2010JCLI3377.1

Edwards, T. L., Nowicki, S., Marzeion, B., Hock, R., Goelzer, H., Seroussi, H., et al. (2021). Projected land ice contributions to twenty-first-century sea level rise. *Nature*, *593*(7857), 74–82. https://doi.org/10.1038/s41586-021-03302-y

Gent, P. R., & Mcwilliams, J. C. (1990). Isopycnal mixing in Ocean circulation models. *Journal of Physical Oceanography*, *20*(1), 150–155. https://doi.org/10.1175/1520-0485(1990)020<0150:IMIOCM>2.0.CO;2

Gent, P. R., Willebrand, J., McDougall, T. J., & McWilliams, J. C. (1995). Parameterizing eddy-induced tracer transports in Ocean circulation models. *Journal of Physical Oceanography*, *25*(4), 463–474. https://doi.org/10.1175/1520-0485(1995)025<0463:PEITTI>2.0.CO;2

Gray, A. R., & Riser, S. C. (2014). A global analysis of Sverdrup balance using absolute geostrophic velocities from Argo. *Journal of Physical Oceanography*, *44*(4), 1213–1229. https://doi.org/10.1175/JPO-D-12-0206.1

Gutierrez-Villanueva, M. O., Chereskin, T. K., & Sprintall, J. (2023). Compensating transport trends in the Drake Passage frontal regions yield no acceleration in net transport. *Nature Communications*, *14*(1), 7792. https://doi.org/10.1038/s41467-023-43499-2

Haid, V., Timmermann, R., Gürses, Ö., & Hellmer, H. H. (2023). On the drivers of regime shifts in the Antarctic marginal seas, exemplified by the Weddell Sea. *Ocean Science*, *19*(6), 1529–1544. https://doi.org/10.5194/os-19-1529-2023

Haigh, M., & Holland, P. R. (2024). Decadal variability of ice-shelf melting in the Amundsen Sea driven by sea-ice freshwater fluxes. Retrieved from https://www.authorea.com/doi/full/10.22541/essoar.170593860.09639068/v1?commit=d1955109cc9e531d9552edd75e9a97c618e80bd5

Hallberg, R. (2013). Using a resolution function to regulate parameterizations of oceanic mesoscale eddy effects. *Ocean Modelling*, *72*, 92–103. https://doi.org/10.1016/j.ocemod.2013.08.007

Hogg, A. M. C. (2010). An Antarctic Circumpolar Current driven by surface buoyancy forcing. *Geophysical Research Letters*, *37*(23). https://doi.org/10.1029/2010GL044777

Hogg, A. M. C., & Gayen, B. (2020). Ocean gyres driven by surface buoyancy forcing. *Geophysical Research Letters*, *47*(16), e2020GL088539. https://doi.org/10.1029/2020GL088539

Holland, W. R. (1973). Baroclinic and topographic influences on the transport in western boundary currents. *Geophysical Fluid Dynamics*, *4*(3), 187–210. https://doi.org/10.1080/03091927208236095

IOC, SCOR and IAPSO. (2010). *The international thermodynamic equation of seawater—2010: Calculation and use of thermodynamic properties*. Intergovernmental Oceanographic Commission, Manuals and Guides No. 56, (p. 196). UNESCO (English). Retrieved from https://www.teos-10.org/pubs/TEOS-10_Manual.pdf

Jacobs, S. S., Giulivi, C. F., & Dutrieux, P. (2022). Persistent Ross Sea freshening from imbalance West Antarctic ice shelf melting. *Journal of Geophysical Research: Oceans*, *127*(3), e2021JC017808. https://doi.org/10.1029/2021JC017808

Liu, T., Ou, H.-W., Liu, X., Qian, Y.-K., & Chen, D. (2022). The dependence of upper ocean gyres on wind and buoyancy forcing. *Geoscience Letters*, *9*(1), 2. https://doi.org/10.1186/s40562-022-00213-2

Madec, G., Bourdallé-Badie, R., Chanut, J., Clementi, E., Coward, A., Ethé, C., et al. (2019). NEMO ocean engine. https://doi.org/10.5281/zenodo.3878122

Mathiot, P., & Jourdain, N. C. (2023). Southern Ocean warming and Antarctic ice shelf melting in conditions plausible by late 23rd century in a high-end scenario. *Ocean Science*, *19*(6), 1595–1615. https://doi.org/10.5194/os-19-1595-2023

Moorman, R., Morrison, A. K., & McC. Hogg, A. (2020). Thermal responses to Antarctic ice shelf melt in an eddy-rich global ocean–sea ice model. *Journal of Climate*, *33*(15), 6599–6620. https://doi.org/10.1175/JCLI-D-19-0846.1

Morrison, A. K., Hogg, A. M., & Ward, M. L. (2011). Sensitivity of the Southern Ocean overturning circulation to surface buoyancy forcing: Southern Ocean overturning. *Geophysical Research Letters*, *38*(14). https://doi.org/10.1029/2011GL048031

Morrison, A. K., Huneke, W. G. C., Neme, J., Spence, P., Hogg, A. M., England, M. H., & Griffies, S. M. (2023). Sensitivity of Antarctic shelf waters and abyssal overturning to local winds. *Journal of Climate*, *36*(18), 6465–6479. https://doi.org/10.1175/JCLI-D-22-0858.1

Neme, J., England, M. H., Hogg, A. M., Khatri, H., & Griffies, S. M. (2023). The role of bottom friction in mediating the response of the Weddell Gyre circulation to changes in surface stress and buoyancy fluxes. *Journal of Physical Oceanography*, *54*(1), 217–236. https://doi.org/10.1175/JPO-D-23-0165.1

Olbers, D., Willebrand, J., & Eden, C. (2012). *Ocean dynamics*. Springer. https://doi.org/10.1007/978-3-642-23450-7

Ong, E. Q. Y., England, M. H., Doddridge, E., & Constantinou, N. C. (2025). Transient Antarctic slope current response to climate change including meltwater. *Geophysical Research Letters*, *52*(10), e2024GL113983. https://doi.org/10.1029/2024GL113983

Park, Y.-H., Park, T., Kim, T.-W., Lee, S.-H., Hong, C.-S., Lee, J.-H., et al. (2019). Observations of the Antarctic Circumpolar Current over the Udintsev Fracture Zone, the narrowest choke point in the Southern Ocean. *Journal of Geophysical Research: Oceans*, *124*(7), 4511–4528. https://doi.org/10.1029/2019JC015024

Patmore, R. D. (2019). *Topographic control of Southern Ocean gyres and the Antarctic Circumpolar Current*. University of Southampton.

Purich, A., & England, M. H. (2021). Historical and future projected warming of Antarctic Shelf Bottom Water in CMIP6 models. *Geophysical Research Letters*, *48*(10). https://doi.org/10.1029/2021GL092752

Shi, J.-R., Talley, L. D., Xie, S.-P., Liu, W., & Gille, S. T. (2020). Effects of buoyancy and wind forcing on Southern Ocean climate change. *Journal of Climate*, *33*(23), 10003–10020. https://doi.org/10.1175/JCLI-D-19-0877.1

Shi, J.-R., Talley, L. D., Xie, S.-P., Peng, Q., & Liu, W. (2021). Ocean warming and accelerating Southern Ocean zonal flow. *Nature Climate Change*, *11*(12), 1090–1097. https://doi.org/10.1038/s41558-021-01212-5

Si, Y., Stewart, A. L., & Eisenman, I. (2023). Heat transport across the Antarctic Slope Front controlled by cross-slope salinity gradients. *Science Advances*, *9*(18), eadd7049. https://doi.org/10.1126/sciadv.add7049

Sonnewald, M., Reeve, K. A., & Lguensat, R. (2023). A Southern Ocean supergyre as a unifying dynamical framework identified by physics-informed machine learning. *Communications Earth & Environment*, *4*(1), 1–20. https://doi.org/10.1038/s43247-023-00793-7

Stewart, A. L. (2021). Warming spins up the Southern Ocean. *Nature Climate Change*, *11*(12), 1–2. https://doi.org/10.1038/s41558-021-01227-y

Stommel, H. (1948). The westward intensification of wind-driven ocean currents. *Transactions - American Geophysical Union*, *29*(2), 202. https://doi.org/10.1029/TR029i002p00202

Sverdrup, H. U. (1947). Wind-Driven currents in a baroclinic Ocean; with application to the equatorial currents of the Eastern Pacific. *Proceedings of the National Academy of Sciences*, *33*(11), 318–326. https://doi.org/10.1073/pnas.33.11.318

Talbot, M. H. (1988). Oceanic environment of George VI Ice Shelf, Antarctic Peninsula. *Annals of Glaciology*, *11*, 161–164. https://doi.org/10.3189/S0260305500006480

Vaughan, D. G., Comiso, J. C., Allison, I., Carrasco, J., Kaser, G., Kwok, R., et al. (2013). Observations: Cryosphere. In *Climate change 2013: The physical science Basis. Contribution of Working Group I to the fifth assessment report of the intergovernmental Panel on climate change*. Cambridge University Press.

Visbeck, M., Marshall, J., Haine, T., & Spall, M. (1997). Specification of Eddy transfer coefficients in coarse-resolution Ocean circulation models. *Journal of Physical Oceanography*, *27*(3), 381–402. https://doi.org/10.1175/1520-0485(1997)027<0381:SOETCI>2.0.CO;2

Wilson, E. A., Thompson, A. F., Stewart, A. L., & Sun, S. (2022). Bathymetric control of subpolar gyres and the overturning circulation in the Southern Ocean. *Journal of Physical Oceanography*, *1*(aop), 205–223. https://doi.org/10.1175/JPO-D-21-0136.1

World of Change: Antarctic Sea Ice. (2009). [Text.Article]. https://earthobservatory.nasa.gov/world-of-change/sea_ice_south.php